



OPEN

Safety and biodistribution of intrathecal administration of mesenchymal stem cells (MSCs) and neurotrophin-releasing nanoparticles in a porcine CSF-guided delivery model for amyotrophic lateral sclerosis (ALS) drug discovery

Emilia Sinderewicz¹, Maria Dąbkowska⁴, Anna Sarnowska², Joanna Staszkiwicz-Chodor¹, Dorota Mystkowska¹, Piotr Holak³, Igor Drozd⁶, Magdalena Chodkowska-Michalowska², Monika Rytel², Edyta Paczkowska⁵, Marcin P. Mycko⁶, Boguslaw Machalinski⁵ & Katarzyna Jezierska-Wozniak^{1,6}✉

Amyotrophic lateral sclerosis (ALS) is a multifactorial neurodegenerative disorder that complicates the identification of effective therapeutic targets. The potential of stem cells and neurotrophins as promising candidates has become increasingly evident, owing to their neuroprotective and anti-inflammatory properties. In this study, a preclinical evaluation of the safety and biodistribution of mesenchymal stromal/stem cells (MSCs) combined with neurotrophin-releasing polyelectrolyte nanoparticles (NTs) was conducted in a porcine intrathecal delivery model relevant to ALS therapy development. Four groups of male pigs were administered saline with NTs, adipose-derived stem cells (ASCs) with NTs, Wharton's jelly-derived MSCs (WJ-MSCs) with NTs, or spinal puncture only. The safety of the treatment was assessed using magnetic resonance imaging (MRI), haematological and biochemical analyses, cerebrospinal fluid profiling, and histology. No adverse effects or significant systemic alterations were observed. It is noteworthy that C-reactive protein levels diminished following NT and NT-MSC administration, suggesting a systemic anti-inflammatory effect. The migration of MSCs was facilitated by cerebrospinal fluid, leading to their accumulation around the spinal cord and brain parenchyma. The present findings demonstrate short-term safety and biodistribution patterns following intrathecal administration of MSCs combined with neurotrophin-releasing nanoparticles in a large-animal model. These preliminary observations provide a pilot framework for future efficacy studies in disease-specific ALS models. This work establishes a translational platform for the development of future ALS therapies, with subsequent studies focused on efficacy testing in disease-

specific models that more accurately reflect the slow, heterogeneous, multisystem nature of human ALS.

Keywords Cell therapy, Stem cells/Mesenchymal stromal cells, Neurotrophin-3, Brain-derived neurotrophic factor, Preclinical studies, Porcine animal model

¹Stem Cell Research Laboratory, Faculty of Medicine, University of Warmia and Mazury, Warszawska 30, Olsztyn 10-082, Poland. ²Translational Platform for Regenerative Medicine, Mossakowski Medical Research Institute, Polish Academy of Sciences, Pawinskiego 5, Warsaw 02-106, Poland. ³Department of Surgery and Radiology with Clinic, Faculty of Veterinary Medicine, University of Warmia and Mazury, Olsztyn 10-719, Poland. ⁴Department of Pharmacokinetics, Biopharmaceutics and Drug Delivery Systems, Pomeranian Medical University, Szczecin 71-899, Poland. ⁵Department of General Pathology, Pomeranian Medical University, Szczecin, Poland. ⁶Department of Neurology and Neurosurgery, Faculty of Medicine, University of Warmia and Mazury, Warszawska 30, Olsztyn 10-082, Poland. ✉ email: katarzyna.jezierska@uwm.edu.pl

Amiotrophic lateral sclerosis (ALS) is driven by multiple mechanisms, including oxidative stress, mitochondrial dysfunction, RNA metabolism defects, neuroinflammation, protein aggregation, and impaired autophagy¹. Non-neuronal cells such as astrocytes, microglia, and immune cells also contribute, either protectively or harmfully². This complexity hinders the identification of unique therapeutic targets. Current drugs, riluzole and edaravone, offer only modest, short-term benefits, with no significant improvement in survival or disease course³. Hence, developing effective therapies remains urgent. Ongoing trials focus on genetic, immune-targeting, and stem cell approaches⁴.

Mesenchymal stem/stromal cells (MSCs) show promise due to their ability to act on multiple pathways simultaneously, modulating immunity, reducing oxidative stress, and promoting regeneration. They have been explored in various neurological disorders⁵. Preclinical ALS studies have tested MSCs from sources such as bone marrow, adipose tissue, and umbilical cord, using intravenous, intrathecal, or spinal injections⁶. Rodent ALS models, especially SOD1 (superoxide dismutase 1) G93A transgenics, replicate key disease features, including motor neuron degeneration and paralysis⁷. However, interspecies differences highlight the need for more adequate large-animal models to better evaluate MSC safety, biodistribution, dosing, and efficacy. In recent years, pigs have become an important preclinical model for ALS, using both transgenic and CNS (central nervous system) injury models⁸. Transgenic pigs with SOD1 and TDP-43 mutations show a disease course resembling human ALS⁹. SOD1G93A pigs develop motor neuron degeneration, hindlimb deficits, gliosis, and protein aggregation in an age-dependent manner¹⁰. Early stages feature nuclear accumulation and ubiquitinated aggregates of mutant SOD1, similar to human ALS pathology¹¹. Later stages show elevated TDP-43 (TAR DNA-binding protein 43) in blood cells and severe skeletal muscle pathology, including inflammation and necrosis¹⁰. Preclinical trials of ALS therapies in animal models demonstrated that stem cell transplantation is feasible and safe, regardless of delivery route, cell type, or dose. However, they showed limited or no functional improvement.

Stem cell-based approaches are among the innovative strategies in ALS therapy research. Another promising direction is the use of neurotrophins, particularly brain-derived neurotrophic factor (BDNF), which supports neuronal survival, differentiation, synapse formation, and provides antioxidant protection during inflammation and hypoxia¹². BDNF acts mainly through TrkB (tropomyosin receptor kinase B) receptors, triggering signaling cascades crucial for cell survival. Neurotrophin-3 (NT3) further enhances BDNF activity by engaging additional Trk receptors¹³. Early ALS trials with methionyl-BDNF showed initial promise, but phase III results were disappointing due to poor protein stability, rapid degradation in circulation, and insufficient delivery across the blood–brain barrier, resulting in no significant clinical benefit¹⁴. To overcome these barriers, nanotechnology-based delivery systems such as PAMAM nanoparticles, multilayer polyelectrolytes, and PEG (Polyethylene Glycol)-based carriers have been developed^{15–17}.

Given the limitations of existing models, the present study was designed as a pilot safety and biodistribution assessment rather than an efficacy investigation. In light of the urgent need for ALS therapies, the unique properties of MSCs, and the limitations of neurotrophins alone, this study aimed to test the combined use of MSCs and neurotrophin-releasing polyelectrolyte nanoparticles in a pig model. Safety and tolerability of intrathecal administration of Wharton's Jelly-derived MSCs (WJ-MSCs), adipose-derived stem cells (ASCs), and nanoparticles were evaluated through *in vivo* experiments, monitoring adverse effects, biochemical markers, cell biodistribution, and procedural outcomes in pigs - a species considered highly relevant for translation to human trials.

Results

Physicochemical characterization of PEGylated NT3-BDNF nanoparticles (NTs)

Physicochemical characterization is a fundamental step in the biological evaluation of nanoparticles, as it is essential for defining or confirming their properties under specific conditions and within a given medium. These properties include object size and its distribution, aggregation and agglomeration states, surface area, surface charge, and solubility. A comprehensive assessment of these characteristics is essential for understanding the interactions of nanoparticles within biological systems and ensuring their safe and effective application. Accordingly, PEGylated NT3-BDNF nanoparticles were comprehensively analyzed using transmission electron microscopy (TEM) to determine their hydrodynamic diameter in a dry state (Fig. 1B), while multiangle dynamic light scattering (MADLS) was utilized to measure their particle size in a PBS solution (Fig. 1C).

Regulatory agencies such as the FDA (Food and Drug Administration) and EMA (European Medicines Agency) require injectable formulations to meet stringent standards for particle size and distribution. A

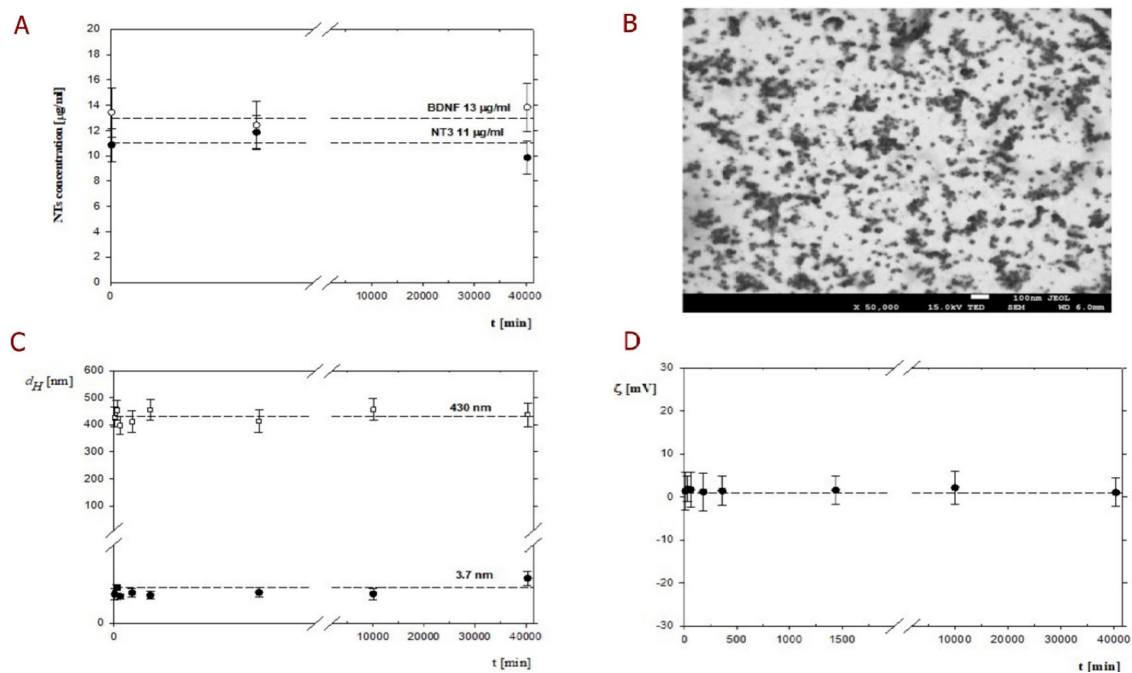


Fig. 1. Physicochemical characterization of PEGylated NT3-BDNF nanoparticles over 28 days (40 320 min) after formulation. **(A)** Loading efficiency of BDNF (open circles) and NT3 (filled circles) in PEGylated NT3-BDNF nanoparticles, determined by ELISA. **(B)** Representative TEM image of PEGylated NT3-BDNF nanoparticles deposited 24 h after formulation (magnification 50,000x; scale bar is 100 nm), showing a dispersed morphology maintained throughout the 28-day period. **(C)** Time-dependent changes in the hydrodynamic diameter (d_H) of PEGylated NT3-BDNF nanoparticles measured by MADLS. The peak intensity data (open and filled points) correspond to the same nanoparticle population and reveal a bimodal size distribution, reflecting both smaller and larger particle fractions. The d_H values were calculated from the Stokes–Einstein equation at pH 7.4 and ionic strength 0.15 M (293 K). Individual points indicate nanoparticle diameter distributions obtained from eight independent samples. **(D)** Zeta potential (ζ) of the nanoparticles measured in PBS buffer and calculated using Henry's equation at an ionic strength of 0.15 M. Dashed lines serve as visual guides. All syntheses were performed in six replicates, and error bars represent mean \pm standard deviation (SD).

polydispersity index (PDI) greater than 0.4 is typically unacceptable unless justified and mitigated through additional formulation strategies. The characteristic hydrodynamic diameter of the PEGylated NT3-BDNF nanoparticles obtained from MADLS studies with concentrations of each neurotrophin (ca. 13.2 mg L⁻¹) was between 3.7 nm \pm 1 nm, and 430 nm \pm 3 nm, indicating a polydispersity index (PDI) (0.38 \pm 0.02).

Additionally, we determined the physicochemical parameters of the synthesized PEGylated nanoparticles and the loading of neurotrophins (NT3 and BDNF) within 90 days of freezing using MADLS (Multi-Angle Dynamic Light Scattering) and ELISA (enzyme-linked immunosorbent assay) (Fig. 1C, and A). TEM (Transmission Electron Microscopy) and MADLS studies indicated that the diameter of the PEGylated NT3-BDNF nanoparticles was between 4 nm and 430 nm, and the polydispersity index was lower than 0.4 after 28 days of freezing. The average concentration of NT-3 and BDNF reached constant values of 11 mg L⁻¹ and 13 mg L⁻¹, respectively, over 28 days of storage. Afterward, the electrophoretic mobility/zeta potential of PEGylated NT3-BDNF nanoparticles was physicochemically characterized (Fig. 1D) to confirm the electrostatic interactions underlying nanoparticle formation. Initially, the individual components exhibited opposite surface charges: NT3 was a positively charged (5 mV \pm 2.5 mV)¹⁶, whereas PEG macroions were negatively charged (-4 mV \pm 2.5 mV)¹⁷. The adsorption of negatively charged PEG onto NT3 reduced the net electrokinetic potential, producing slightly positive PEG-NT3 conjugates (+ 3.6 \pm 3.2 mV). Subsequent adsorption of mildly negatively charged BDNF (-0.66 \pm 1.91 mV) onto PEG-NT3 complexes further decreased the surface charge, yielding PEGylated NT3-BDNF nanoparticles with a ζ potential of + 1.33 \pm 4.79 mV. This progressive charge compensation supports the formation of the nanoparticles through electrostatic coupling among PEG, NT3, and BDNF molecules. Microelectrophoretic measurements demonstrated that the ζ potential of the resulting PEGylated NT3-BDNF nanoparticles remained stable throughout the 28-days of observation, confirming colloidal stability of the formulation.

Analysis of biochemical parameters and blood morphology

Due to the limited sample size ($n = 3$ per group) and the exploratory nature of this safety study, the hematological and biochemical data were not subjected to inferential statistical testing. The descriptive presentation reflects

the methodological constraints and prevents over-interpretation of numerical variability that may not represent biologically meaningful effects.

The analysis of selected biochemical parameters and blood counts on smears from the experimental animals was performed in an accredited veterinary laboratory on samples collected at four time points: before the first administration of cells/NaCl (1), one week after the first administration of cells/NaCl (2), one week after the second administration of cells/NaCl (3), one week after the administration of NTs (4). The results are presented in the Table 1.

There were single, small deviations from the norm (both before and during the treatments), but their nature was scattered and irregular. In the control group, two of three animals had temporarily elevated levels of leukocytes and neutrophils - these values returned to normal after at least the third administration of NaCl. An increased number of thrombocytes was also observed in one animal, which also normalized after the third administration of NaCl. The remaining individual deviations were close to the limit values and therefore, given the lack of statistical analysis, cannot be considered biologically significant. In the control group, transient elevations in leukocyte and neutrophil counts were noted in two of the three animals. These values returned to the reference range by at least the third NaCl administration. One animal also exhibited an elevated thrombocyte count, which normalized following the third NaCl dose. Other deviations from reference intervals were minimal and remained close to threshold values.

In the WJ-MSc group, all animals demonstrated a mild reduction in MCH, with values remaining near the lower reference limit throughout the study. In one animal, a slight reduction in monocyte count persisted across timepoints, and an increase in eosinophil count was observed prior to the third and fourth administrations. Remaining deviations were infrequent and of small magnitude.

In the ASC group, minor reductions in MCH and MCV were observed at all examined timepoints. One animal presented with a reduced eosinophil count before and after the first cell administration, which returned to normal after NTs administration. Another animal showed deviations in leukocyte, monocyte, and AST levels before and shortly after the first administration; these parameters later stabilized within reference ranges. One animal died before study completion; however, no indication of a procedure-related cause was identified based on available clinical observations.

In the sham-operated group, slight deviations in MCH and MCV were observed throughout the experiment. One animal demonstrated markedly elevated ALT levels; because elevated ALT was present both pre-procedure and during the study, this finding was not attributed to experimental interventions.

C-reactive protein level

C-reactive protein (CRP) levels were measured in plasma (Fig. 2) and cerebrospinal fluid (Fig. 3) of pigs within three examined groups: (1) control group, (2) group of pigs receiving intrathecal ASC, (3) group of pigs receiving intrathecal WJ-MSc, at four time points of the experiment: 0: before the start of cells/NaCl administration, I: one week after the first administration of cells/NaCl, II: one week after the second administration of cells/NaCl, III: one week after NTs administration.

Subsequent to the primary administration of cells/NaCl (time point I), a statistically significant increase in plasma CRP levels was observed in the control ($p < 0.01$) and WJ-MSc ($p < 0.0001$) groups, whereas no significant change was observed in the ASC group. Following the second administration (time point II), a significant decrease in CRP levels was observed in the WJ-MSc groups ($p < 0.001$), while no significant change was detected in the control and ASC groups. The administration of NT (time point III) resulted in a decrease in CRP levels in all groups; however, a further statistically significant decrease was only observed in the ASC group. This decline was statistically significant ($p < 0.01$) in the ASC and WJ-MSc groups, and ($p < 0.05$) in the control group.

In the ensuing week following the initial administration (time point I), a substantial increase in CSF CRP levels was observed exclusively within the control group ($p < 0.05$). At this juncture, no other significant changes were detected in the cell-injected groups. Subsequent to the second administration of the cell (time point II), no statistically significant differences were observed among the groups. The NT administration (time point III) resulted in a decrease in CSF CRP levels in all groups; however, this decrease was statistically significant ($p < 0.01$) in the cell-injected groups.

Tissue staining

HE staining was used to assess the preservation of tissue and cell integrity. Analysis of the images obtained showed no deviation from the norm. Anatomical structures were preserved and the tissues contained many normal cells. Figure 4 shows examples of the structures analysed. The analysed specimens come from the brain and spinal cord of a pigs treated with WJ-MSc and neurotrophins.

Representative micrographs showing preserved cytoarchitecture and intact cellular morphology with no evidence of tissue damage or inflammatory infiltration. Panels B I–B IV correspond to different regions of the brain: I – section near the cerebralventricle; II – lateralcerebralcortex; III – region adjacent to the medulla oblongata; IV – dorsal (upper) section. Representative spinal cord (SC) sections were obtained from the thoracic level (T11).

The assessment of iron staining intensity was qualitative and based on the Visual evaluation of Prussian blue Signac under identical imaging parameters (light intensity, magnification, and contrast). Two independent observers blinded to group allocation performed the evaluation. Unstained sections and tissues from NaCl-treated animals served as negative controls to verify staining specificity and background signal.

Staining with potassium ferrocyanide confirmed the presence of trivalent iron, which was used to label the administered cells (Fig. 5). As a result of this staining, iron ions took on a dark blue color. In order to assess the degree of MSCs deposition labeled with iron ions in the nervous system tissues during the analysis of images

| Parameter | Unit | Standard range | NaCl/NTs | | | | ASC/NTs | | | | WJ-MSC/NTs | | | | Sham operated | | | | | |
|--------------|---------------------|----------------|----------|---------|----------|----------|---------|---------|----------|----------|------------|---------|----------|----------|---------------|---------|----------|----------|-------|----|
| | | | Day 0 | Day 7th | Day 14th | Day 21st | Day 0 | Day 7th | Day 14th | Day 21st | Day 0 | Day 7th | Day 14th | Day 21st | Day 0 | Day 7th | Day 14th | Day 21st | | |
| MCV | fl | 50-68 | n=1 | 49,7 | 50,5 | 49,9 | 50,8 | 50,3 | 50,1 | | 49 | 49,9 | 49,2 | 49,3 | 49,6 | 52,3 | 51,8 | | 51,8 | |
| | | | n=2 | 50,1 | 49 | 49,1 | 50 | 49,7 | 49,5 | | 48 | 51 | 50,7 | 50,2 | 50,5 | 45,7 | 44,8 | | 45,8 | |
| | | | n=3 | 46,9 | 48 | 47,9 | 48,2 | 44,3 | 43,8 | | AD | 47,5 | 46,9 | 47,1 | 47,4 | AD | AD | AD | AD | AD |
| | | | Average | 48,9 | 49,17 | 48,97 | 49,67 | 48,1 | 47,8 | | 48,5 | 49,47 | 48,93 | 48,87 | 49,17 | 49 | 48,3 | | 48,8 | |
| MCH | pg | 17-23 | n=1 | 16 | 16 | 15,9 | 15,7 | 16,2 | 16,5 | | 16 | 15,8 | 15,8 | 15,8 | 15,8 | 16,3 | 16,5 | | 16,2 | |
| | | | n=2 | 15,6 | 15,7 | 15,7 | 15,8 | 15,2 | 15,4 | | 15,3 | 16,6 | 16,4 | 16 | 16,3 | 14,8 | 14,7 | | 14,8 | |
| | | | n=3 | 15,8 | 15,6 | 15,6 | 15,4 | 14,4 | 14 | | AD | 14,8 | 14,9 | 15,2 | 15,5 | AD | AD | AD | AD | |
| | | | Average | 15,80 | 15,77 | 15,73 | 15,63 | 15,27 | 15,3 | | 15,65 | 15,73 | 15,7 | 15,67 | 15,87 | 15,55 | 15,6 | | 15,5 | |
| MCHC | g/dl | 30-34 | n=1 | 32,2 | 31,7 | 31,8 | 30,9 | 32,2 | 33 | | 32,6 | 31,7 | 32 | 32,1 | 31,9 | 31,1 | 31,9 | | 31,3 | |
| | | | n=2 | 31,3 | 32 | 31,9 | 31,7 | 30,6 | 31,1 | | 31,9 | 32,5 | 32,4 | 31,9 | 32,3 | 32,5 | 32,8 | | 32,3 | |
| | | | n=3 | 33,7 | 32,5 | 32,5 | 31,9 | 32,6 | 31,9 | | AD | 31,2 | 31,7 | 32,3 | 32,7 | AD | AD | AD | AD | |
| | | | Average | 32,4 | 32,07 | 32,07 | 31,5 | 31,8 | 32 | | 32,25 | 31,8 | 32,03 | 32,1 | 32,3 | 31,8 | 32,35 | | 31,8 | |
| Erythrocytes | mln/ul | 5-8 | n=1 | 5,47 | 6,53 | 7,05 | 6,45 | 6,55 | 6,63 | | 6,97 | 7,24 | 6,47 | 6,8 | 7,25 | 7,09 | 6,9 | | 7,27 | |
| | | | n=2 | 6,6 | 7,06 | 7,47 | 6,61 | 7,73 | 7,67 | | 7,93 | 6,9 | 6,65 | 6,69 | 6,64 | 7,63 | 6,75 | | 7,93 | |
| | | | n=3 | 7,19 | 6,95 | 7,87 | 7,04 | 6,86 | 7,36 | | AD | 7,07 | 6,51 | 7,43 | 6,94 | AD | AD | AD | AD | |
| | | | Average | 6,42 | 6,85 | 7,46 | 6,7 | 7,05 | 7,22 | | 7,45 | 7,07 | 6,54 | 7,47 | 6,94 | 7,36 | 6,83 | | 7,6 | |
| Hematocrit | % | 32-50 | n=1 | 27,2 | 33 | 35,2 | 32,8 | 32,9 | 33,2 | | 34,1 | 36,1 | 31,8 | 33,5 | 36 | 37,1 | 35,7 | | 37,7 | |
| | | | n=2 | 33 | 34,6 | 36,7 | 33 | 38,4 | 38 | | 38,1 | 35,2 | 33,7 | 33,6 | 33,6 | 34,8 | 30,2 | | 36,3 | |
| | | | n=3 | 33,7 | 33,3 | 37,7 | 33,9 | 30,4 | 32,2 | | AD | 33,6 | 30,5 | 35 | 32,9 | AD | AD | AD | AD | |
| | | | Average | 31,3 | 33,63 | 36,53 | 33,23 | 33,9 | 34,47 | | 36,1 | 34,97 | 32 | 34,03 | 34,17 | 35,95 | 32,95 | | 37 | |
| Hemoglobin | g/dl | 10-16 | n=1 | 8,7 | 10,4 | 11,2 | 10,1 | 10,6 | 11 | | 11,1 | 11,4 | 10,2 | 10,8 | 11,5 | 11,5 | 11,4 | | 11,8 | |
| | | | n=2 | 10,3 | 11,1 | 11,7 | 10,5 | 11,8 | 11,8 | | 12,1 | 11,4 | 10,9 | 10,7 | 10,8 | 11,3 | 9,9 | | 11,7 | |
| | | | n=3 | 11,4 | 10,8 | 12,2 | 10,8 | 9,9 | 10,3 | | AD | 10,5 | 9,7 | 11,3 | 10,8 | AD | AD | AD | AD | |
| | | | Average | 10,13 | 10,77 | 11,7 | 10,47 | 10,77 | 11,03 | | 11,6 | 11,1 | 10,27 | 10,93 | 11,03 | 11,4 | 10,65 | | 11,75 | |
| Leukocytes | x10 ⁹ /l | 10-20 | n=1 | 41,15 | 42,42 | 20,52 | 18,86 | 16,87 | 18,12 | | 18,96 | 15,45 | 18,75 | 12,63 | 16,76 | 11,13 | 15,53 | | 12,55 | |
| | | | n=2 | 20,77 | 26,46 | 23,66 | 14,87 | 9,86 | 8,89 | | 12,89 | 16,88 | 13,06 | 14,83 | 14,3 | 17,93 | 20,11 | | 14,78 | |
| | | | n=3 | 15 | 19,21 | 20,77 | 14,16 | 13,5 | 8,67 | | AD | 17,26 | 16,43 | 19,32 | 12,21 | AD | AD | AD | AD | |
| | | | Average | 25,64 | 29,36 | 21,65 | 15,96 | 13,41 | 11,89 | | 15,93 | 16,53 | 16,08 | 15,59 | 14,42 | 14,53 | 17,82 | | 13,67 | |
| Thrombocytes | G/l | 200-520 | n=1 | 932 | 540 | 629 | 417 | 414 | 296 | | 287 | 404 | 492 | 496 | 361 | 243 | 421 | | 199 | |
| | | | n=2 | 353 | 527 | 310 | 346 | 497 | 431 | | 376 | 465 | 365 | 403 | 355 | 304 | 391 | | 126 | |
| | | | n=3 | 237 | 733 | 556 | 291 | 538 | 564 | | AD | 552 | 483 | 504 | 548 | AD | AD | AD | AD | |
| | | | Average | 507,33 | 600 | 498,33 | 351,33 | 483 | 430,33 | | 331,5 | 473,67 | 446,67 | 467,67 | 421,33 | 273,5 | 406 | | 162,5 | |
| Neutrophils% | % | 26,6-56,7 | n=1 | 67,3 | 63,8 | 52,9 | 47,1 | 36,4 | 35,5 | | 49,3 | 34,9 | 48,8 | 43,2 | 37,4 | 30,9 | 47,5 | | 31,5 | |
| | | | n=2 | 60,2 | 55,1 | 49,9 | 35,6 | 34,7 | 31,8 | | 47,6 | 41,1 | 50,5 | 53,5 | 37,3 | 43,1 | 60,3 | | 38,4 | |
| | | | n=3 | 46,5 | 49,9 | 59,1 | 38,1 | 33,6 | 39,7 | | AD | 50,4 | 48,4 | 66 | 33,1 | AD | AD | AD | AD | |
| | | | Average | 58 | 56,27 | 53,97 | 40,27 | 34,9 | 35,67 | | 48,45 | 42,13 | 49,23 | 54,23 | 35,93 | 37 | 53,9 | | 34,95 | |
| Lymphocytes% | % | 35,5-62 | n=1 | 28,3 | 31 | 43,1 | 45,5 | 53,8 | 45,2 | | 46,1 | 61,2 | 46,9 | 49,3 | 57,3 | 58,6 | 45,7 | | 52,4 | |
| | | | n=2 | 35,1 | 39 | 43,7 | 57,9 | 60,4 | 60,6 | | 47,3 | 55,4 | 43,5 | 38,2 | 49,5 | 52,8 | 34,3 | | 54,2 | |
| | | | n=3 | 47,6 | 43,7 | 36,9 | 56 | 62,3 | 52 | | AD | 45,4 | 45 | 29 | 61,3 | AD | AD | AD | AD | |
| | | | Average | 37 | 37,9 | 41,23 | 53,13 | 58,83 | 52,6 | | 46,7 | 54 | 45,13 | 38,83 | 56,03 | 55,7 | 40 | | 53,3 | |
| Monocytes% | % | 1,6-8,8 | n=1 | 2,2 | 2,5 | 1,7 | 2,8 | 2,8 | 3,6 | | 1,9 | 2 | 1,7 | 1,4 | 2,5 | 2,2 | 2,6 | | 1,6 | |
| | | | n=2 | 3,1 | 3,7 | 2,8 | 2,7 | 1,5 | 1,8 | | 1,9 | 1,5 | 1,8 | 1,2 | 2 | 1,6 | 2,5 | | 1,1 | |
| | | | n=3 | 2,6 | 3,6 | 2,1 | 1,9 | 1,5 | 4,4 | | AD | 2,3 | 5,1 | 2,6 | 2,9 | AD | AD | AD | AD | |
| | | | Average | 2,63 | 3,27 | 2,2 | 2,47 | 1,93 | 3,27 | | 1,9 | 1,93 | 2,87 | 1,73 | 2,47 | 1,9 | 2,55 | | 1,35 | |
| Eosinophils% | % | 0,5-6 | n=1 | 1,1 | 1,4 | 1,2 | 2,2 | 6,1 | 14,3 | | 1,8 | 0,8 | 1 | 4,9 | 2,2 | 7 | 2,8 | | 13,3 | |
| | | | n=2 | 0,7 | 1,4 | 2,3 | 3 | 2,1 | 4,3 | | 1,8 | 1 | 2 | 5,9 | 10,6 | 1,2 | 2,2 | | 4,8 | |
| | | | n=3 | 2 | 1 | 0,9 | 2,6 | 1,5 | 1,5 | | AD | 0,6 | 0,6 | 1,6 | 1,1 | AD | AD | AD | AD | |
| | | | Average | 1,27 | 1,27 | 1,47 | 2,6 | 3,23 | 6,7 | | 1,8 | 0,8 | 1,2 | 4,13 | 4,63 | 4,1 | 2,5 | | 9,05 | |
| Basophils% | % | 0,2-7 | n=1 | 0,5 | 0,5 | 0,7 | 1,5 | 0,7 | 0,6 | | 0,4 | 0,6 | 0,4 | 0,4 | 0,3 | 0,7 | 0,3 | | 0,4 | |
| | | | n=2 | 0,6 | 0,6 | 0,5 | 0,7 | 0,7 | 0,7 | | 0,4 | 0,6 | 0,4 | 0,5 | 0,4 | 0,7 | 0,4 | | 0,8 | |
| | | | n=3 | 0,7 | 0,7 | 0,7 | 0,8 | 0,5 | 0,7 | | AD | 0,7 | 0,7 | 0,6 | 0,6 | AD | AD | AD | AD | |
| | | | Average | 0,60 | 0,60 | 0,63 | 1,00 | 0,63 | 0,67 | | 0,4 | 0,63 | 0,5 | 0,5 | 0,43 | 0,7 | 0,35 | | 0,6 | |
| Neutrophils | x10 ⁹ /l | 3,1-9,6 | n=1 | 27,68 | 27,07 | 10,85 | 8,88 | 6,14 | 6,42 | | 9,34 | 5,4 | 9,16 | 5,46 | 5,14 | 3,43 | 7,37 | | 3,95 | |
| | | | n=2 | 12,5 | 14,57 | 11,81 | 5,3 | 3,42 | 2,82 | | 6,14 | 6,94 | 6,59 | 7,93 | 5,33 | 7,72 | 12,13 | | 5,68 | |
| | | | n=3 | 6,98 | 9,59 | 12,28 | 5,39 | 4,54 | 3,44 | | AD | 8,7 | 7,95 | 12,75 | 4,04 | AD | AD | AD | AD | |
| | | | Average | 15,72 | 17,08 | 11,65 | 6,52 | 4,7 | 4,23 | | 7,74 | 7,01 | 7,9 | 8,71 | 4,84 | 5,58 | 9,75 | | 4,82 | |
| Lymphocytes | x10 ⁹ /l | 4,6-10 | n=1 | 11,64 | 13,13 | 8,83 | 8,58 | 9,07 | 8,2 | | 8,74 | 9,45 | 8,8 | 6,23 | 7,88 | 6,52 | 7,09 | | 6,58 | |
| | | | n=2 | 7,29 | 10,31 | 10,35 | 8,61 | 5,96 | 5,39 | | 6,1 | 9,36 | 5,69 | 5,67 | 7,08 | 9,47 | 6,89 | | 8,01 | |
| | | | n=3 | 7,14 | 8,39 | 7,67 | 7,93 | 8,4 | 4,51 | | AD | 7,84 | 7,38 | 5,61 | 7,49 | AD | AD | AD | AD | |
| | | | Average | 8,69 | 10,61 | 8,95 | 8,37 | 7,81 | 6,03 | | 7,42 | 8,88 | 7,29 | 5,84 | 7,48 | 8,00 | 6,99 | | 7,30 | |
| Monocytes | x10 ⁹ /l | 0,3-1,2 | n=1 | 0,92 | 1,04 | 0,35 | 0,52 | 0,48 | 0,65 | | 0,37 | 0,31 | 0,33 | 0,18 | 0,35 | 0,24 | 0,4 | | 0,21 | |
| | | | n=2 | 0,65 | 0,97 | 0,66 | 0,4 | 0,14 | 0,16 | | 0,24 | 0,25 | 0,23 | 0,18 | 0,29 | 0,28 | 0,51 | | 0,16 | |
| | | | n=3 | 0,4 | 0,7 | 0,44 | 0,28 | 0,2 | 0,38 | | AD | 0,39 | 0,84 | 0,5 | 0,35 | AD | AD | AD | AD | |
| | | | Average | 0,66 | 0,90 | 0,48 | 0,4 | 0,27 | 0,40 | | 0,31 | 0,32 | 0,47 | 0,29 | 0,33 | 0,26 | 0,46 | | 0,19 | |
| Eosinophils | x10 ⁹ /l | 0,001-0,9 | n=1 | 0,45 | 0,61 | 0,26 | 0,42 | 1,03 | 2,59 | | 0,35 | 0,13 | 0,19 | 0,62 | 0,3 | 0,78 | 0,44 | | 1,67 | |
| | | | n=2 | 0,16 | 0,38 | 0,55 | 0,44 | 0,21 | 0,38 | | 0,23 | 0,17 | 0,26 | 0,88 | 1,51 | 0,22 | 0,45 | | 0,71 | |
| | | | n=3 | 0,3 | 0,2 | 0,19 | 0,37 | 0,2 | 0,13 | | AD | 0,11 | 0,1 | 0,31 | 0,14 | AD | AD | AD | AD | |
| | | | Average | 0,30 | 0,40 | 0,33 | 0,41 | 0,48 | 1,03 | | 0,29 | 0,14 | 0,18 | 0,60 | 0,65 | 0,5 | 0,45 | | 1,19 | |
| Basophils | x10 ⁹ /l | 0-0,5 | n=1 | 0,19 | 0,21 | 0,14 | 0,29 | 0,13 | 0,11 | | 0,08 | 0,1 | 0,08 | 0,06 | 0,05 | 0,08 | 0,05 | | 0,05 | |
| | | | n=2 | 0,12 | 0,15 | 0,13 | 0,1 | 0,06 | 0,06 | | 0,06 | 0,1 | 0,05 | 0,08 | 0,06 | 0,12 | 0,07 | | 0,11 | |
| | | | n=3 | 0,1 | 0,14 | 0,14 | 0,11 | 0,07 | 0,06 | | AD | | | | | | | | | |

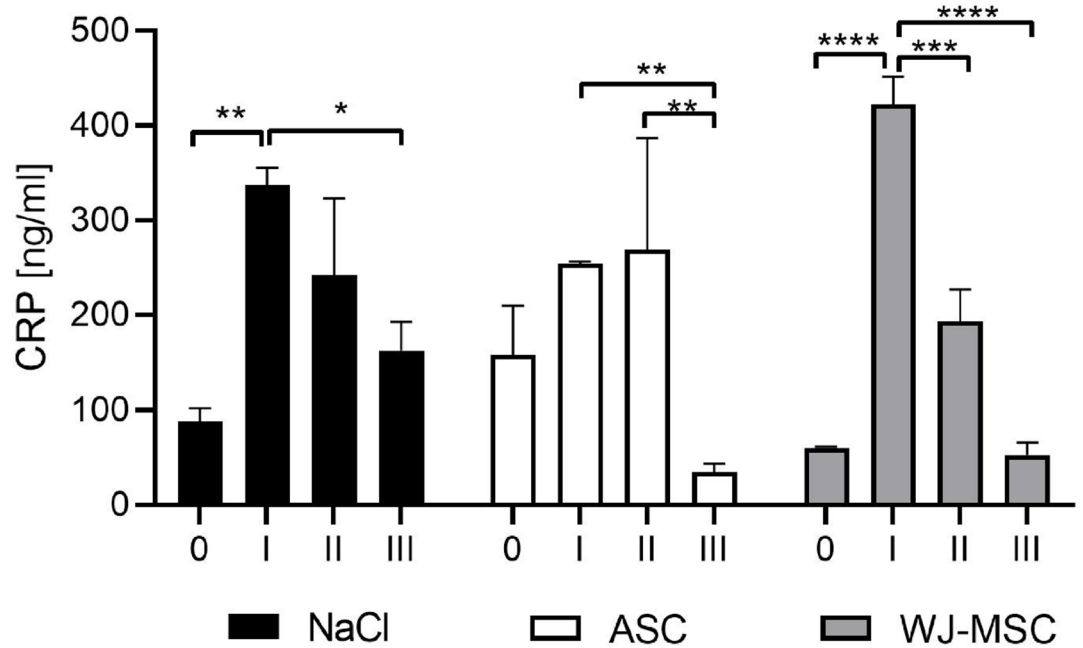


Fig. 2. CRP concentration in plasma of the pigs receiving NaCl (control group, black bars), pigs receiving ASC (white bars), pigs receiving WJ-MSC (grey bars) in a four timepoints of the experiment: O: pre-1st cells/NaCl administration, I: post-1st cells/NaCl administration, II: post-2st cells/NaCl administration, III: one week after NTs administration. Data are presented as mean \pm SD ($n = 3$ per group). Due to the small sample size, individual data points are not displayed. The statistical analysis was determined by a two-way ANOVA followed by Tukey's multiple comparison test ($p < 0.05$). Asterisks indicate differences in the CRP concentration between examining timepoints (* $p < 0.05$, ** $p < 0.01$, *** $p < 0.001$, **** $p < 0.0001$).

obtained as a result of potassium ferrocyanide staining, the signal strength was marked with numerical values (1–4; 1 means a weak signal in the form of few iron deposits, and 4 means a strong signal in the form of very numerous iron deposits). Analysis of histological slides from the animals' spinal cords showed the greatest presence of iron ions at the site of administration and its nearest area (end thoracic and lumbar, Figs. 5, 6 and 7). The qualitative assessment of Prussian blue staining indicated weak to moderate signal intensity surrounding the spinal cord and ventricular regions in animals receiving labeled MSCs. The presence of trivalent iron was also observed in the terminal part of the spinal cord and brain, indicating the migration of labelled cells with the circulating intracellular fluid. In animals brain preparations, the highest concentrations of iron ions were found in fragments located at the periphery of the tissue on the side of the ventricles and on the side of the medulla oblongata (Figs. 5 and 6). No penetration of the administered cells through the blood-brain barrier into the tissues was observed (Fig. 5). This result suggests that the presence and action of MSCs is local. Below there are sample images of the structures analysed showing staining for trivalent iron. The specimens analysed were taken from the brain and spinal cord of a pig treated with WJ-MSC and neurotrophins. Since a qualitative analysis of the obtained images was used, the results presented at Fig. 6 are intended to indicate the CNS fragments in which iron ion deposits were identified, but not to statistically assess the signal strength between the analyzed CNS sections or between experimental groups.

A semi-quantitative scoring system was not applied because the staining intensity varied substantially between tissue blocks and was influenced by technical factors inherent to Prussian blue staining. Combined with the small sample size, this precluded reliable statistical comparisons. Therefore, the assessment was restricted to a qualitative, observer-blinded evaluation focusing on the spatial distribution of iron-labelled cells.

MRI

The analysis of MRI images after MSC/NTs administration was compared with images obtained before the start of the administration procedure. In control animals, no changes were observed in any MRI sequences (T2-TSE-COR, T2-TSE-SAG, T2-FL2D-SAG-HEMO, T2-TSE-TRA, T2-SPC-SAG-ISO-1.0MM) after placebo administration compared to pre-surgery images (Fig. 8A). In images acquired before the start of cell/NaCl administration, no artifacts were detected in the spinal canal.

MRI images from animals that received MSC/NTs in the operating room and were subsequently transported to the MRI laboratory also showed no artifacts (Fig. 8B–E), likely due to dilution and redistribution of cells in the cerebrospinal fluid during transport.

In contrast, images acquired during intrathecal cell administration under MRI guidance revealed localized hypointense signals on T2-weighted sequences (T2-TSE-COR, T2-TSE-SAG, T2-TSE-TRA), characteristic of

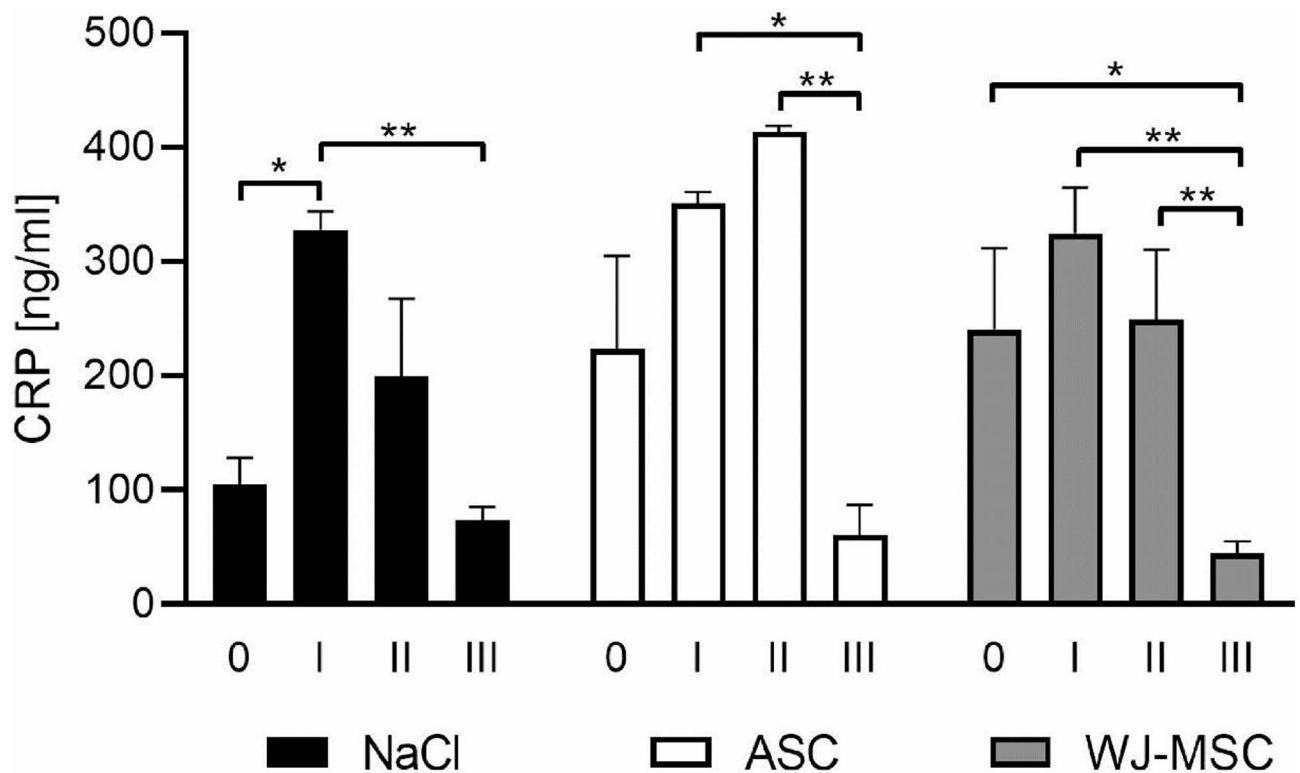


Fig. 3. CRP concentration in CSF of the pigs receiving NaCl (control group, black bars), pigs receiving ASC (white bars), pigs receiving WJ-MSC (grey bars) in a four timepoints of the experiment: 0: pre-1st cells/NaCl administration, I: post-1st cells/NaCl administration, II: post-2nd cells/NaCl administration, III: CRP decreased after the second administration of NaCl, while in the ASC group it remained at the same level one week after NTs administration (III). Data are presented as mean \pm SD ($n=3$ per group). Due to the small sample size, individual data points are not displayed. The statistical analysis was determined by a two-way ANOVA followed by Tukey's multiple comparison test ($p < 0.05$). Asterisks indicate differences in the CRP concentration between examining timepoints (* $p < 0.05$, ** $p < 0.01$, *** $p < 0.001$, **** $p < 0.0001$).

iron-labeled cells (Fig. 9A–D). These signals were observed approximately 10 cm above the drain insertion site, consistent with the recorded drain length, confirming the location of administered cells within the spinal canal.

No MRI changes were observed in animals receiving cells postoperatively after transport, nor in control animals after placebo administration (Fig. 8A–E). MRI images acquired one week after the last surgical procedures showed no alterations in the spinal canal in any study group. Throughout the experiment, animal caretakers did not report any deviations from normal health, supporting the safety of the intrathecal administration method.

Discussion

In recent years, research interest in cell therapies as a potential approach to treating neurological diseases has increased substantially due to their multifactorial mechanisms. In this context, the present work should be viewed as a pilot study focused on assessing the safety and biodistribution of MSCs and neurotrophin-releasing nanoparticles in healthy pigs, without evaluating their therapeutic efficacy. Current ALS treatments, such as riluzole and edaravone, dopaminergic drugs used in Parkinson's disease, and immunomodulators for multiple sclerosis (MS), mainly provide symptomatic relief, have limited overall efficacy, and often produce adverse effects¹⁸. Despite advances in neuroprotective agents and gene therapies, their long-term effectiveness remains uncertain. These limitations, particularly in rare disorders such as ALS, highlight the need for strategies that can regenerate neural tissue and support functional recovery, with stem cell-based interventions representing a promising avenue.

Initially, MSCs were expected to differentiate into neural cells and replace damaged motor neurons. However, later studies showed their main role is regulating the microenvironment by releasing neurotrophic factors and cytokines that modulate immune responses¹⁹. This supports activation of endogenous cells, stimulates neurogenesis and angiogenesis, and reduces secondary cell death through anti-inflammatory effects^{20,21}. Administration of hUCB (human umbilical cord blood) was shown to decrease reactive gliosis and slow disease progression, while SCF (stem cell factor)-activated bone marrow cells improved motor function and survival in ALS mice by lowering pro-inflammatory cytokines and increasing IGF-1 (insulin-like growth factor)²². These findings highlight the importance of modifying the CNS microenvironment and suggest that supplementing stem cell therapy with additional trophic factors may enhance its effectiveness in ALS treatment.

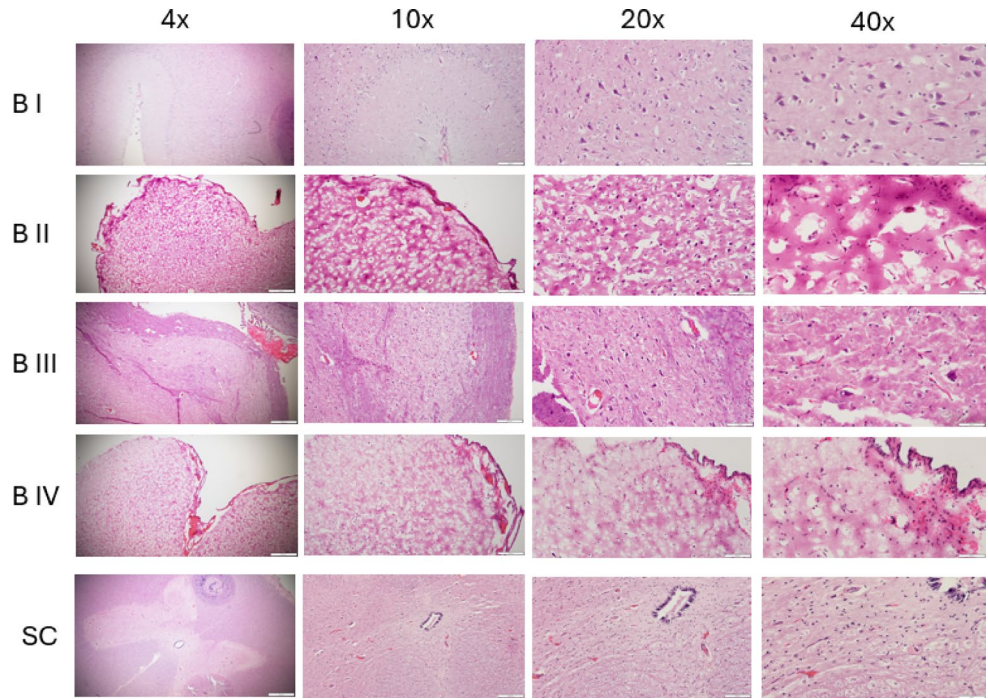


Fig. 4. Hematoxylin and eosin (HE) staining of the brain and spinalcord of pigstreated with Wharton’sJelly-derived mesenchymal stem cells (WJ-MSCs) and neurotrophins.

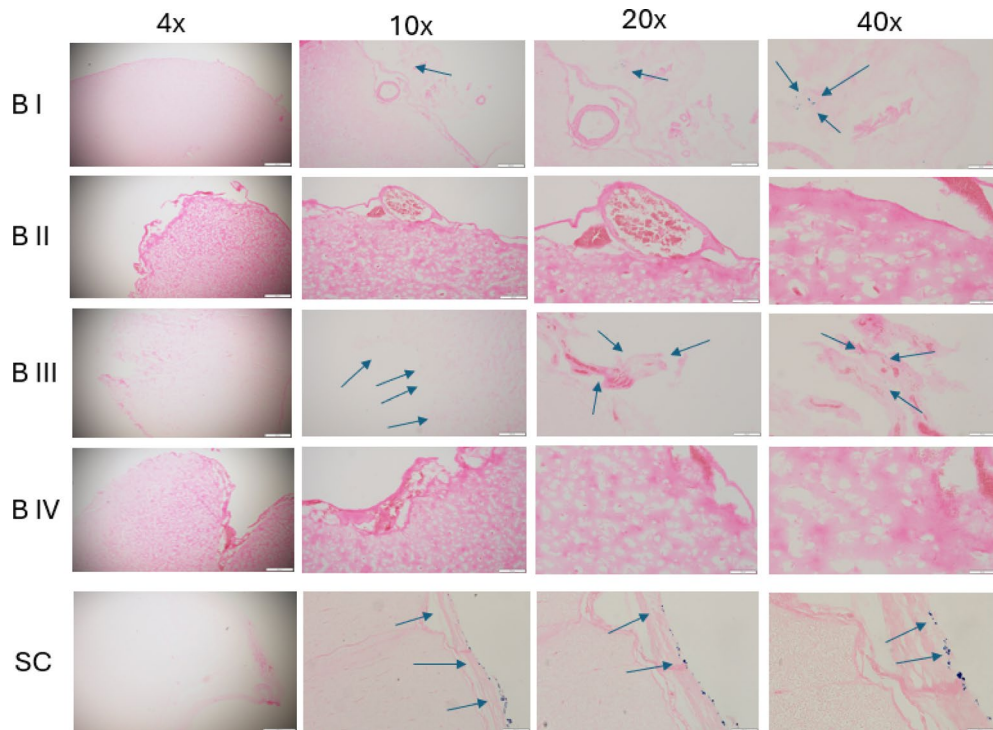


Fig. 5. The staining withpotassium ferrocyanide of brain and spinal cord of a pigs treated with WJ-MSC and neurotrophins. B I – B IV denote the following brain fragments: section I - cut from the side of the cerebral ventricle, section II from the lateral side, section III from the side of the medulla oblongata and section IV from the top. The examples of spinal cord (SC) tissue originate from the thoracic section (T11). 4x, 10x, 20x, 40x - symbols indicating the magnification factor. Iron deposition is indicated by blue arrows.

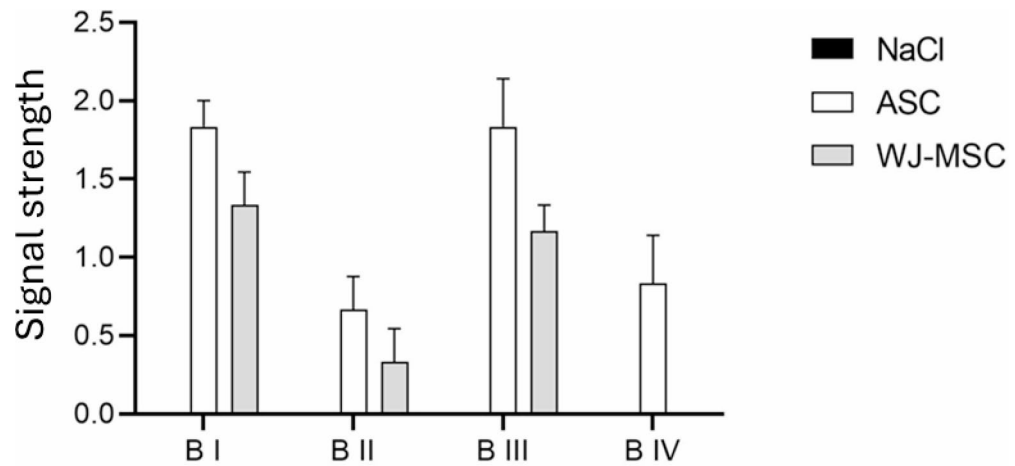


Fig. 6. Distribution of iron-labelled mesenchymal stem/stromal cells (MSCs) in the brain of pigs after intrathecal administration. Graph showing the qualitative assessment of iron-labelled MSC deposition in different brain regions of pig receiving NaCl (black bars), adipose-derived stem cells (ASC; white bars), or Wharton'sJelly-derived MSCs (WJ-MSC; grey bars). BI–BIV denote the analyzed brain areas: I – ventricular region, II – lateral cerebral cortex, III – region adjacent to the medulla oblongata, IV – dorsal (upper) brain section. The Y-axis indicates signal strength (arbitrary units, qualitative scale 1–4; 1 = weak, 4 = strong) corresponding to the intensity of Prussian-blue staining for trivalent iron. Each value represents the mean qualitative score obtained independently by two blinded observers under identical imaging parameters. Values represent qualitative scores only; no statistical comparison was performed.

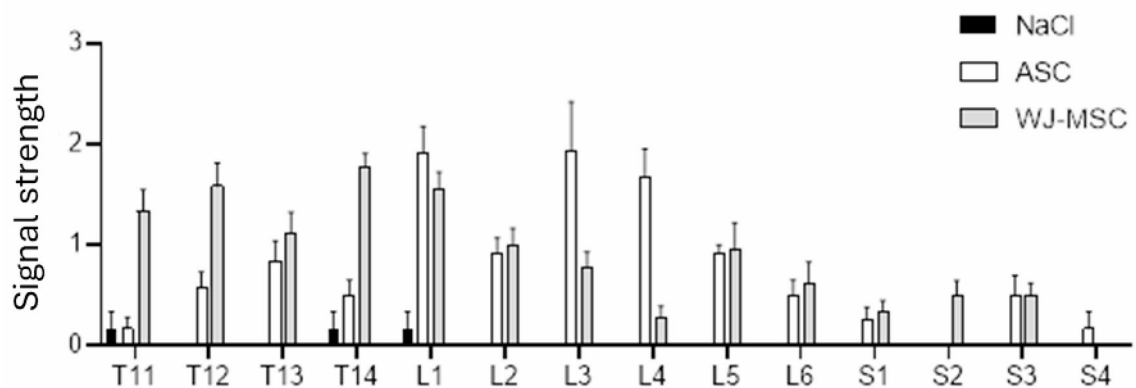


Fig. 7. Distribution of iron-labelled mesenchymal stem/stroma cells (MSCs) in the spinal cord of pigs after intrathecal administration. Graph showing the qualitative assessment of iron-labelled MSC deposition along the spinal cord in pig receiving NaCl (black bars), adipose-derived stem cells (ASC; white bars), or Wharton'sJelly-derived MSCs (WJ-MSC; Grey bars). T11–T14 correspond to thoracic spinal cord segments, L1–L5 to lumbar segments, and S1–S4 to sacra segments. The Y-axis indicates signal strength (arbitrary units, qualitative scale 1–4; 1 = weak, 4 = strong) representing the relative intensity of Prussian-blue staining. Higher signal values indicate a greater presence of iron deposits, confirming local accumulation of labeled MSCs around the spinal cord. Values represent qualitative scores only; no statistical comparison was performed.

Preclinical animal models have shown that a number of stem cell types could be viable options for ALS therapy. These include autologous BM and adipose-derived MSCs, Wharton's jelly-derived MSCs, granulocyte colony-stimulating factor (G-CSF)-stimulated peripheral blood stem cells (PBSCs), embryonic stem cells (ESCs), NPCs (neural progenitor cells) derived from fetal or adult tissues, and non-neural progenitor cells (non-NPCs)²³. However, the optimal type for human testing remains unclear²⁴. Early clinical trials have assessed the safety and potential efficacy of various stem cell sources and delivery methods, from intravenous and intra-arterial to intrathecal, intraspinal, and intracerebral administration²³. Considering ALS heterogeneity and expert

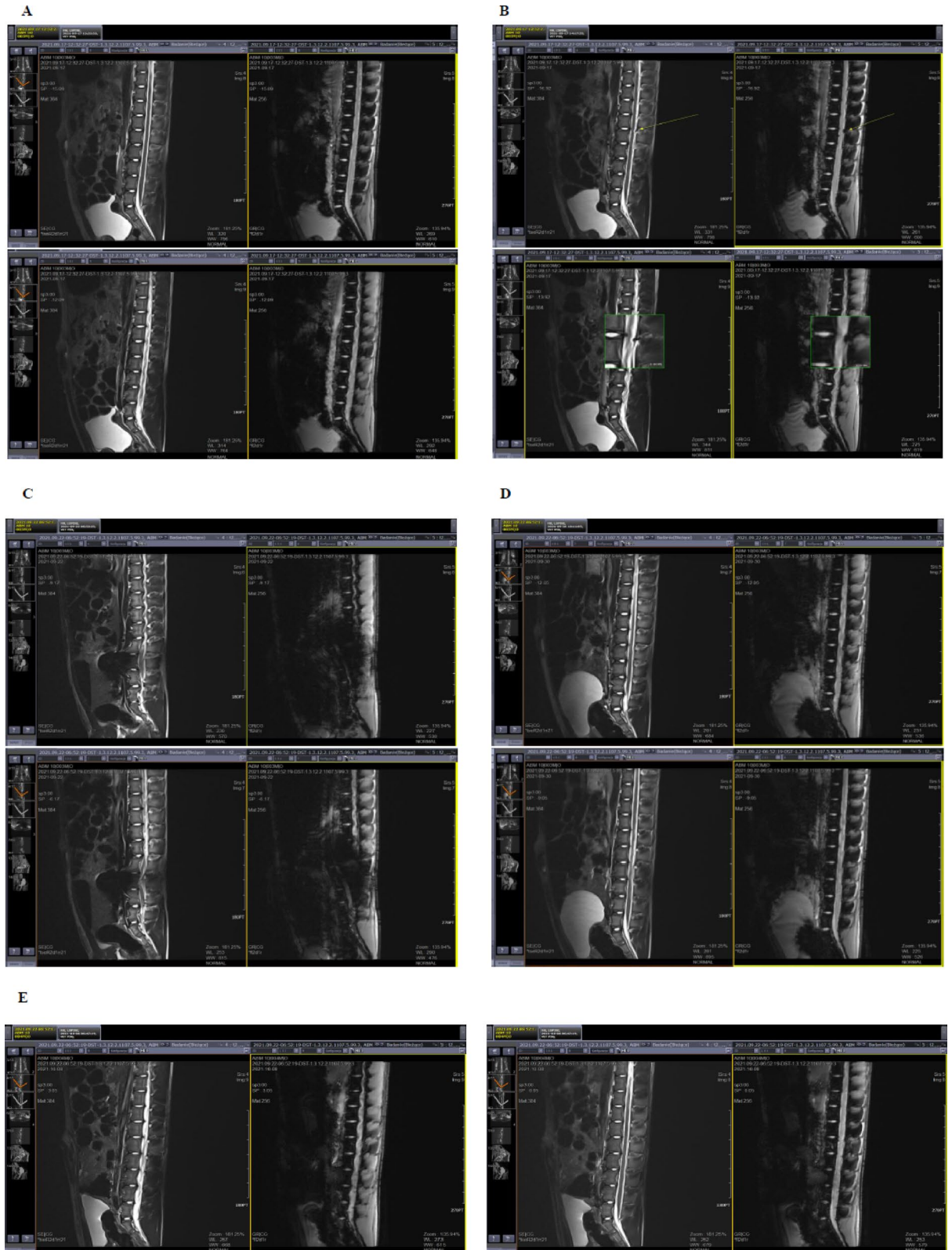


Fig. 8. MRI visualization of intrathecal administration of mesenchymal stem/stromal cells (MSCs) and neurotrophin-releasing nanoparticles in pigs. Representative sagittal T2-weighted MRI images obtained at different stages of the experiment: (A) baseline scan before any intervention, showing normal spinal canal appearance without artefacts; (B) immediately after the first intrathecal administration of MSCs/NaCl, with arrows indicating the injection site and cerebrospinal fluid space; (C) one week after the second administration, showing no pathological signal changes; (D) after neurotrophin (NTs) administration, showing mild hypointense signal in the spinal canal corresponding to iron-labelled MSCs suspended in cerebrospinal fluid; (E) one week after the final procedure, showing complete normalization and absence of hypointense artefacts.

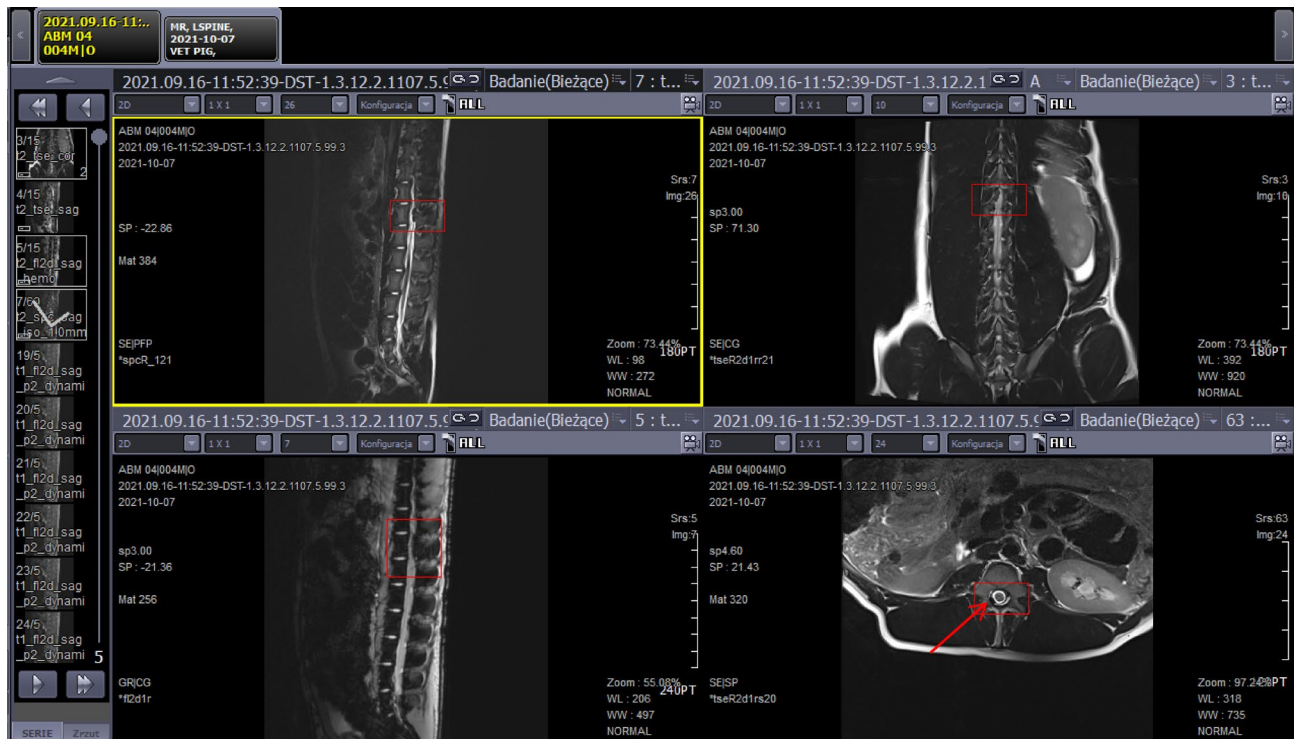


Fig. 9. MRI detection of iron-labelled Wharton's Jelly-derived mesenchymal stem cells (WJ-MSCs) in the cerebrospinal fluid after intrathecal infusion. MRI images obtained during and after cell administration showing characteristic hypointense areas (marked by red arrows and frames) corresponding to iron-labelled cells. (A) Sagittal plane view showing the localization of the signal approximately 10 cm above the drain insertion site; (B) coronal plane confirming the spatial distribution of the signal within the spinal canal; (C) sagittal plane with hemo-expansion sequence allowing enhanced visualization of iron-related hypointensity; (D) transverse plane demonstrating cross-sectional localization of the signal within the cerebrospinal fluid compartment. The hypointense areas correspond to the presence of superparamagnetic iron-labelled MSCs, confirming their localization within the subarachnoid space and the absence of pathological changes in surrounding tissues.

recommendations²⁵, we chose intrathecal administration of allogenic ASC and MSC, avoiding long autologous preparation times and the need for immunosuppression.

Clinical studies frequently use MSCs as the therapeutic cell source. Safety has been demonstrated for BM-MSCs, WJ-MSCs, ASCs, and neural stem cells (NSCs)^{26–30}. Phase I trials of intraspinal NSI-566RSC NSCs (lumbar or cervical) reported good tolerability and occasional ALSFRS-R stabilization, particularly at higher doses^{26,31}. Intraparenchymal NSC delivery was also safe and associated with transient slowing of disease progression²⁸. Repeated intrathecal or intravenous BM-MSC administration demonstrated safety and reductions in inflammatory markers, although efficacy remained inconclusive due to small cohorts^{32–34}. Phase II IT BM-MSC trials showed dose-interval-dependent clinical benefit³⁰. Repeated IT WJ-MSC administration prolonged median survival without serious adverse events³⁵. Intrathecal autologous ASC injections were well tolerated, causing only minor CSF alterations and nerve root thickening; subjective improvements were reported, though ALSFRS-R scores remained unchanged³⁶.

This study employed both adipose-derived MSCs (ASC/AD-MSC) and Wharton's jelly MSCs (WJ-MSC) to explore their safety and biodistribution in the context of neuroregenerative therapy. Both cell types possess properties relevant to neurological applications: AD-MSCs have demonstrated neuroprotective, anti-inflammatory, and neurogenic effects in central nervous system disorders, while WJ-MSCs produce a diverse secretome with paracrine factors that support neuronal survival and tissue repair. Including both sources allowed us to evaluate potential differences in *in vivo* behavior, persistence, and interaction with neurotrophin-releasing nanoparticles, providing a broader perspective on MSC-based strategies for neurological applications. Future studies may further investigate functional outcomes, secretome profiles, and immunological responses to optimize cell selection and therapeutic design³⁷.

Previous studies indicate that stem cells may play a beneficial role in ALS therapy, although their efficacy remains uncertain. In this context, our work focuses on evaluating the safety and feasibility of combining MSCs with neurotrophin-releasing nanoparticles rather than assessing therapeutic outcomes. Intrathecal and intramuscular autologous BM-MSCs have been reported to slow disease progression by increasing neurotrophic factors and reducing inflammatory CSF biomarkers in rapidly progressing patients, although some trials did not reach statistical significance³⁸. Preclinical research has also explored MSCs combined with neurotrophin-

releasing nanoparticles in pigs to enhance therapeutic potential. Considering both effectiveness and minimal invasiveness, the intrathecal route was selected for delivering cells and neurotrophins.

The primary safety assessment involved monitoring animal health before, during, and after the procedures. No behavioral abnormalities suggesting deterioration were reported. Hematological and biochemical parameters remained stable across all timepoints in both control and experimental groups, with no patterns indicating adverse effects. One ASC-treated animal died during recovery from anesthesia after the second administration; post-mortem and histological examinations of the CNS and peripheral organs revealed no procedure- or preparation-related lesions, and the death was attributed to anesthesia. Overall, the absence of relevant changes in measured parameters supports the safety of the approach. Comparable findings have been reported clinically: intrathecal WJ-MSC administration was well tolerated, with only a single case of headache among 34 ALS patients³⁴, and intrathecal autologous BM-MSC injections produced no serious adverse events, aside from occasional mild pyrexia, pain, or headache^{29,39}. Similarly, lumbar puncture-based MSC delivery showed no procedure-related complications³². Given the link between ALS and neuroinflammation, CRP levels in plasma and cerebrospinal fluid were measured at baseline (before the first administration), after the first administration, and after the second administration. In all groups, a transient increase in CRP was observed after the first administration, which likely reflected a short-term inflammatory response to the procedure. Following the second administration, CRP levels decreased toward baseline values in all groups. However, these post-administration fluctuations did not reach statistical significance when compared to pre-administration (baseline) levels, except for the ASC group, where a modest intergroup difference was observed ($p < 0.05$). Thus, the observed CRP dynamics primarily reflect transient procedural effects rather than treatment-specific inflammatory changes.

Our findings are in accordance with phase III of the clinical trial findings also revealed significant improvements in cerebrospinal biomarkers of neuroinflammation, neurodegeneration, and neurotrophic factor support in patients who received three intrathecal MSC-NTF treatments. The treatment was well tolerated but did not reach statistical significance⁴⁰. Moreover, it was documented, that injections of MSCs and Lin- cells, isolated from bone marrow, induce the secretion of neurotrophic factor and diminish the inflammation in ALS patients³⁸. Although CRP is a non-specific systemic inflammatory marker, it was selected in this study to monitor acute inflammatory responses after intrathecal administration of cells and nanoparticles in a large-animal model. CRP was selected as a general indicator of systemic and cerebrospinal inflammation associated with the intrathecal procedure and administration of MSCs or nanoparticles. Although it is a non-specific marker, it is widely used to monitor acute inflammatory responses and procedural safety in large-animal preclinical studies. Changes in CRP concentration provide insight into transient immune activation and overall tolerability of the applied treatment. The short-term fluctuations in CRP levels are more likely to be a consequence of a transient inflammatory response to the procedure, rather than a disease-related effect. Consequently, the observed normalization of CRP following neurotrophin administration should be interpreted as evidence of safety and procedural tolerability, rather than as a direct therapeutic effect. The conclusions derived from biochemical and hematological parameters must be interpreted cautiously, as the small number of animals limits statistical power. Therefore, the reported observations should be regarded as indicative of safety trends rather than definitive evidence.

It is acknowledged that biomarkers relevant to ALS, such as neurofilament light chain (NfL) or cytokine profiles (IL-6, TNF- α , IL-10), would provide more disease-specific information on neuroinflammation and neurodegeneration. Subsequent studies will incorporate these markers to facilitate a more comprehensive evaluation of the translational and pathophysiological relevance of MSC/NT-based therapies.

Neurotrophins such as BDNF and NT3 were selected for their well-established neuroprotective and anti-inflammatory properties in neurodegenerative diseases, including ALS. Both factors promote neuronal survival, axonal regeneration, and synaptic maintenance; however, their therapeutic use is limited by rapid degradation and a short systemic half-life. To overcome these limitations, PEGylated polyelectrolyte nanoparticles were developed as controlled-release carriers, enabling gradual and sustained neurotrophin delivery. PEGylation enhances nanoparticle stability, reduces immunogenicity, and prolongs protein bioavailability, as demonstrated in our previous *in vitro* and *in vivo* studies, where PEGylated NT3-BDNF albumin-based nanoparticles maintained stable size, electrokinetic properties and provided continuous neurotrophin release for up to 28 days¹⁷. Importantly, compared with cell-based approaches, administration of PEGylated neurotrophin-releasing nanoparticles induces a markedly lower inflammatory response. This likely results from the absence of cellular immunogenic components and the inert character of the PEG coating, which minimizes immune cell recognition and complement activation. Consequently, nanoparticle-based delivery could represent a safer and more controllable strategy for sustained neurotrophin release and modulation of neuroinflammation in ALS therapy. Encapsulation of NT3 and BDNF in PEGylated nanoparticles can also improve their pharmacokinetic properties by enhancing thermal stability, solubility, and bioavailability, while potentially facilitating their passage across the blood-brain barrier. These advantages not only extend the therapeutic window of neurotrophins but also open the possibility of applying such formulations in a broader spectrum of central nervous system disorders, including epilepsy and other neurodegenerative or inflammatory pathologies. The use of natural bioactive molecules within biocompatible nanocarriers, therefore, represents a promising direction for the development of modern and safe neuroprotective therapies.

Our results, obtained in healthy pigs, indicate that the combination of NTs and WJ-MSCs modulated inflammatory markers in CSF without adverse effects. While these findings demonstrate safety and biological activity, any potential neuroprotective or therapeutic implications for ALS remain hypothetical and require validation in disease-specific models. Successful stem cell therapy requires reliable outcome measures, but no *in vivo* assay universally confirms transplantation, incorporation, or neurotrophic factor secretion. Clinical trials track cell fate to ensure safety and prevent migration to undesirable regions⁴¹. To avoid interference with cell biology, we used iron as a contrast agent. Superparamagnetic iron oxide particles (SPIOs) are widely

studied⁴² due to fast labelling, long half-life, and high MRI resolution⁴³. SPIOs do not affect stem cell survival, proliferation, or differentiation⁴⁴. SPIO-labelled cells produce hypointense areas on T2/T2*-weighted MRI, indicating transplanted cell location.

MRI during spinal cord administration showed hypointense areas above the drain site, confirming procedure effectiveness. SPIO-labelled cells, however, cannot be distinguished from hemorrhage or clots⁴⁵. Absence of artefacts in animals transported to MRI suggests signals were not due to hemorrhage. Lack of hypointense signal in animals without a drain likely resulted from cell suspension dispersal in cerebrospinal fluid. An alternative approach may involve the use of gadolinium (Gd-DTPA), fluorine (¹⁹F), or manganese complexes for clearer localization⁴⁶.

Comparing MRI before, during, and one week after procedures showed no spinal canal changes, consistent with previous studies, supporting the safety of intrathecal administration of the prototype medicinal product.

Besides promising therapeutic outcomes, a key consideration in cell therapy is their fate and potential consequences. Human DNA was detected in peripheral organs, but not in the brain after intravenous UCB administration⁴⁷, prompting further studies on IV or CNS delivery. In SOD1G93A mice, few IV hUCB-HSCs reached the spinal cord, while most localized in the spleen, modulating immune response and increasing Th2 cytokines²¹. hUCB-MSCs injected into CSF remained in the subarachnoid space or lateral ventricles, likely secreting neurotrophic and anti-inflammatory factors⁴⁸.

In this study, we evaluated MSC biodistribution and the preservation of CNS tissue and cellular integrity. Consistent with our previous observations, tissue architecture and cellular phenotype remained normal. Iron ions used for MSC labeling were detected around the spinal cord and brain surfaces, with the highest concentrations at the tissue periphery, the ventricular surfaces, and the medulla oblongata. No evidence of MSC penetration across the blood–brain barrier into the parenchyma was observed, indicating that the administered cells remained confined to the cerebrospinal fluid space and exhibited limited distribution without integration into CNS tissue.

These histological findings confirm that the administered MSCs remained in the subarachnoid space without integrating into neural tissue, suggesting their therapeutic effects are primarily paracrine, mediated by neurotrophic factors, cytokines, and extracellular vesicles that modulate inflammation and support neuronal survival rather than direct cell replacement.

Limitations

The present study has several limitations that should be acknowledged:

Animal model and translational relevance

The experiments were performed in healthy pigs to evaluate the safety, biodistribution, and inflammatory response following intrathecal administration of mesenchymal stromal/stem cells (MSCs) combined with neurotrophin-releasing nanoparticles. While this large-animal model provides valuable translational data, it does not reproduce the pathological features of amyotrophic lateral sclerosis (ALS) or other neurodegenerative diseases. Therefore, the findings cannot be directly extrapolated to therapeutic outcomes in patients. Additionally, species-specific physiological differences between pigs and humans may affect biodistribution, immune response, and neurotrophin release kinetics, which should be carefully considered in the context of clinical translation. Only male juvenile animals were included, which may influence physiological and inflammatory parameters.

Sample size and statistical power

The small number of animals per group ($n=3$) limits statistical power and the ability to detect subtle biological effects. The loss of one animal in the ASC group further reduced the available data, although this event was unrelated to treatment. The sample size was determined in accordance with the 3Rs principle (Replacement, Reduction, and Refinement) to minimize animal use while allowing detection of major biological trends. As a result, the current results are primarily descriptive and should be regarded as preliminary.

Follow-up duration

The 21-day follow-up period limits the assessment of long-term safety and persistence of administered cells. This pilot study focused on short-term biodistribution, with iron-based cell labeling optimized for limited monitoring periods.

Histological and analytical limitations

Some histological outcomes, particularly iron staining, were assessed qualitatively rather than quantitatively due to variability in signal intensity, sample characteristics, and the limitations of staining and imaging methods, which did not allow reliable quantification. The small number of replicates further prevented meaningful statistical comparisons between groups; therefore, representative images are provided to illustrate localization, and the results are presented descriptively, focusing on the distribution and relative abundance of iron deposits within CNS regions. These findings confirm cell localization and support the safety and feasibility of intrathecal administration, although therapeutic efficacy cannot be determined in the absence of a disease model. Future studies will incorporate functional, behavioral, and biomarker assessments to evaluate the translational potential of the MSC/NT approach in ALS and related neurodegenerative disorders.

Scope of the present study

This study should be framed as a pilot investigation focused on short-term safety, feasibility of intrathecal administration, and biodistribution tracking. Therapeutic efficacy, disease relevance, long-term safety, and

comprehensive biomarker or functional assessments were not addressed and cannot be inferred from the current data.

Future perspectives

To strengthen the translational relevance of MSC/neurotrophin combination therapy, future studies will need to include larger cohorts, both sexes, and comprehensive functional, behavioral, and biomarker analyses. Long-term follow-up and quantitative histological evaluations will be essential to confirm safety, persistence, and potential therapeutic effects. These aspects will form the focus of subsequent research, building upon the preliminary findings reported here.

Materials and methods

Ethical approval

All methods were conducted in accordance with relevant guidelines and regulations. The study was carried out in strict accordance with the recommendations in the Guide for the Care and Use of Laboratory Animals of the National Institutes of Health. All animal experiments were approved by the Local Ethics Committee in Olsztyn (approval no. 36/2021) and were performed in compliance with the ARRIVE guidelines.

Human mesenchymal stem/stromal cells isolated from Wharton's Jelly of the umbilical cord (WJ-MSC) were obtained under approval of the Bioethics Committee (Resolution no. 27/2015) at the University of Warmia and Mazury in Olsztyn, Poland.

Adipose tissue was collected during the liposuction procedure of Plastic Surgery Department at Orłowski's Clinical Hospital in Warsaw. The study protocol was approved by the Institutional Review Board (IRB) at the Centre of Postgraduate Medical Education (No. 62/PB/2016) on September 14, 2016. All procedures involving human tissue were performed in accordance with relevant guidelines and regulations. Written informed consent was obtained from all donors (or their legal guardians) prior to sample collection.

Proceeding of the in vivo experiment

In order to investigate the safety and tolerance of intrathecal administration of mesenchymal stem/stromal cells (MSC) and biocompatible nanoparticles made of polyelectrolytes releasing neurotrophins (NTs), an in vivo experiment on the animal model was conducted. During the experiment, the tested products were administered intrathecally, in the lumbar section of the spinal canal of pigs, and the number of adverse events, biochemical parameters as well as biodistribution of transplanted cells were analysed.

All procedures were approved by Local Ethics Committee in Olsztyn (approval 36/2021) and were performed in accordance with the ARRIVE guidelines. The experiment was conducted on the 12 castrated male pigs with an average weight of approximately 30 kg. The animals were housed in the animal facility of the Faculty of Veterinary Medicine of the University of Warmia and Mazury in Olsztyn. The light cycle was 12 h on and 12 h off. The rooms were equipped with a continuous and emergency ventilation system with the capacity ensuring 15 to 20 air changes per hour. The noise level did not exceed 60 dB. The air temperature was maintained at 21 Celsius degrees, and the humidity was maintained at a level of 50–60%. The animals were provided with access to a clean place to lie down, drinking water, hay and straw. Following their transportation from the breeder to the animal facility, the boars were subjected to the required adaptation period before the start of the in vivo experiment. The animals were earmarked, divided into four research groups ($n=3$) and placed in the aforementioned pens (3 animals per pen).

The number of animals ($n=3$ per group) was selected based on ethical considerations and previously published large-animal preclinical studies evaluating the safety and biodistribution of stem cell-based therapies. The study was designed as a pilot, exploratory experiment focusing on feasibility and safety rather than hypothesis-driven efficacy testing. Sample size reduction followed the 3Rs principle (Replacement, Reduction, and Refinement) to minimize animal use while maintaining the ability to detect potential adverse effects or inflammatory responses.

In the experiment human mesenchymal stem/stromal cells isolated from Wharton's jelly of the umbilical cord (WJ-MSC; Bioethics Committee Resolution No. 27/2015), human mesenchymal stem/stromal cells isolated from adipose tissue (ASC; Bioethical Committee at the Centre of Postgraduate Medical Education (No. 63/PB/2013) and neurotrophin-releasing nanoparticles (NTs) were used. The tested cells were administered intrathecally twice, at a dose of 5 million, with a seven-day interval between each administration. Seven days following the second administration of cells, the animals were administered 250 μ l of PEGylated NT3-BDNF nanoparticles, containing 13.2 mg L⁻¹ of each neurotrophins. The third group of animals, which served as the control group, was given 0.9% NaCl twice and NTs once, at seven-day intervals. The fourth group was the sham-operated group. This group underwent a spinal canal puncture only, four times at seven-day intervals.

The experimental setup is shown below (Fig. 10).

Prior to each surgical procedure, the animals were premedicated and anaesthetised in the animal facility. Xylazine (Vetaxyl) was administered intramuscularly at a dosage of 3 mg/kg, ketamine intramuscularly at a dosage of 5–8 mg/kg, and atropine (Atropinum sulfuricum WZF 1 mg/mL) subcutaneously at dosage of 0.05 mg/kg. Subsequently, butorphanol (Torbugesic) was administered intravenously at a dosage of 0.3 mg/kg, propofol intravenously at a dosage of 2–4 mg/kg and the animals were intubated. The general anaesthesia was maintained with isoflurane 2–3% by inhalation. After that, the animals were transported to the Emil Behring's Experimental Medicine Centre of the Faculty of Medicine, University of Warmia and Mazury in Olsztyn, in a specially adapted car. Every time, the animals were under the supervision of a veterinarian, with access to life-sustaining/life-saving equipment.

On day 0, a baseline, magnetic resonance imaging (MRI) of the spine of each pig was performed. The examinations were conducted using in T1 and T2 sequences, without contrast administration. During the study, the pigs were anaesthetised with sevoflurane 1–2.5.5% by inhalation. Thereafter, the pigs were then transported

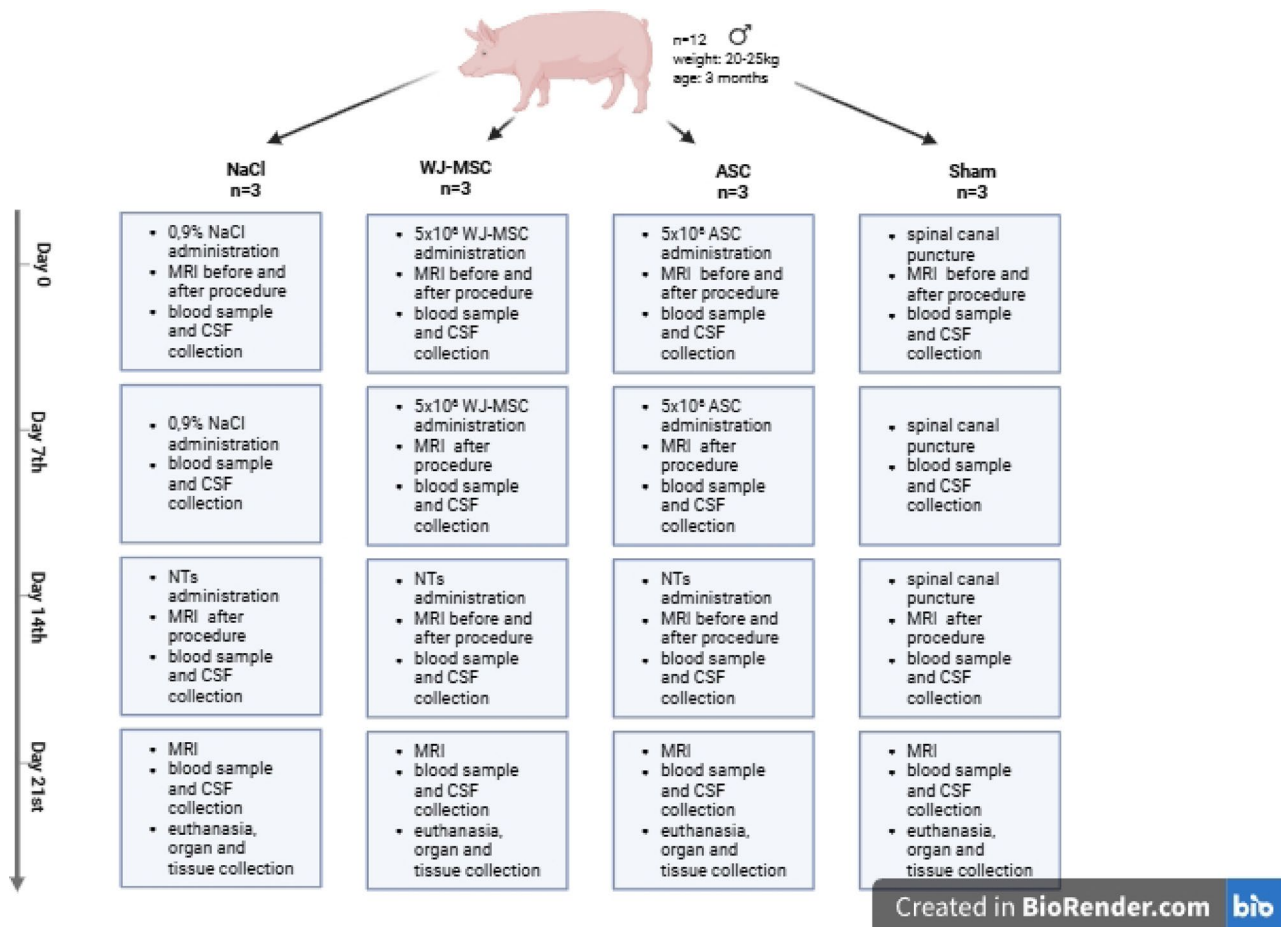


Fig. 10. The scheme of in vivo experiment. Group I: 0.9% NaCl administered intrathecally (i.t.) on day 0 and 7, NTs administered i.t. on day 14, $n = 3$; Group II: ASC administered i.t. on day 0 and 7, NTs administered i.t. on day 14, $n = 3$; Group III: WJ-MSC administered i.t. on day 0 and 7, NTs administered i.t. on day 14, $n = 3$; Group IV: sham operated; $n = 3$. Created with BioRender.com.

to the operating room. The animals were administered intrathecally in the lumbar spine with 0.5 mL of 0.9% NaCl (control group, 1), ASC and WJ-MSC (experimental groups, 2 and 3, respectively; 5 million cells suspended in 0.5 mL of sterile PBS), or only the injection was performed (sham operated group, 4). The procedure was conducted under intraoperative X-ray control. As during MRI, pigs were maintained under anaesthesia with sevoflurane 1–2.5.5% by inhalation. After surgery, the pigs underwent a repeat MRI imaging. After completion of the procedure, the pigs were transported to the animal facility under general anaesthesia and in appropriate conditions, where they were awakened under the veterinary supervision and received the necessary post-operative care. The animals were kept under veterinary supervision for 24 h after the procedure. Biochemical tests were performed on the blood samples, including morphology, alanine aminotransferase (ALT), aspartate aminotransferase (AST) and C-reactive protein (CRP) levels. Additionally, cerebrospinal fluid was collected.

The procedure was repeated after 7 days. Postoperative MRI imaging was performed. After 14 days from the beginning of the experiment, animals in the experimental and control groups received PEGylated NT3–BDNF nanoparticles, containing 13.2 mg L⁻¹ of each neurotrophins suspended in 0.5 mL of sterile PBS, instead of the cells/0.9% NaCl. In the sham-operated group, the injection was repeated. Blood samples for biochemical tests and cerebrospinal fluid were taken each time. MRI of the spine was performed after the procedure. The animals showed no central nervous system damage, pain symptoms or other abnormalities, after any of the treatments, which may confirm the safety of the method used. After a further 7 days (21 days from the start of the experiment), MRI of the spines was repeated. Finally, the animals were euthanized and tissues were collected for assessment of cell biodistribution. Animals were euthanized with pentobarbital (Euthasol vet. 400 mg/ml) administered intravenously at a dose of 140 mg/kg. Brain, spinal cord and fragments of the liver, spleen and lung located near large blood vessels were obtained. The tissues were fixed and frozen until histochemical analyses. The corpses were transferred to the corpse repository at the Department of Pathological Anatomy of the Faculty of Veterinary Medicine of the University of Warmia and Mazury in Olsztyn and then transferred to the rendering plant.

Cell-based product preparation

WJ-MSC, produced in the Laboratory for Regenerative Medicine, Department of Neurosurgery, University of Warmia and Mazury in Olsztyn and ASC obtained from the Mossakowski Medical Research Institute, Polish Academy of Sciences, were thawed and seeded into flasks containing DMEM medium (Macopharma #BC0110060) supplemented with the antibiotic penicillin-streptomycin (Sigma Aldrich #P0781) 2% v/v, Human Platelet Lysate Virally inactivated MultiPL100i (Macopharma #BC0190032) 5% v/v and heparin (Sigma-Aldrich #H3149-250KU) 0.1% v/v. Approximately 18 h before administration, the cells were labelled with Molday ION Rhodamine B iron preparation (BioPAL #CL-50Q02-6 A-50) for magnetic resonance imaging. The preparation was added to the bottles in the amount of 10 $\mu\text{L}/\text{mL}$ of medium. On the day of administration, the cells were detached using trypsin (Sigma-Aldrich #T4049), washed and prepared for administration of 5 million cells suspended in 0.5 mL of sterile PBS for each pig.

NPs preparation

In our earlier work, we studied the PEG layers' self-assembled arrangement¹⁶ in a serum-free and complex serum environment with 0.1, 1, or 5 mg L^{-1} concentrations of both neurotrophins.

The main objective of this research was to produce and characterize PEGylated NT3-BDNF nanoparticles containing 13.2 mg L^{-1} of each BDNF and NT3, with a particular focus on their physicochemical behavior over time in 0.15 M phosphate-buffered saline (PBS) at pH 7.4, and 37 °C. To assess the 28-day stability of the obtained nanoparticles, a set of physicochemical and morphological analyses was performed using transmission electron microscopy (TEM) for structural evaluation and multi-angle dynamic and electrophoretic light scattering (MADLS/ELS) for size distribution and surface charge characterization.

Reagents

BDNF and NT3

Unfiltered stock solutions (typically 250 mg L^{-1}) of carrier-free recombinant human BDNF (rhBDNF) (248-N4-250/CF; R&D Systems, Canada), as well as carrier-free recombinant human NT3 (rhNT3) (248-BDB-250/CF; R&D Systems), were prepared by dissolving lyophilized of known concentrations in phosphate-buffered saline (PBS) (pH 7.4 ± 0.2 , 0.15 M; Biomed, Lublin, Poland) and storing them for no longer than 2 months at -20 °C. In the text, BDNF and NT3 are collectively referred to as neurotrophins (NTs). Before each measurement, the stock solution was diluted to the desired bulk concentration, 10 mg L^{-1} , in Ringer's solution (pH 7.0 ± 0.6 , 0.16 M) (Fresenius Kabi, Polska). The exact concentrations of these solutions were determined by the commercially available enzyme-linked immunosorbent assay (ELISA) (described in 2.3.4). The temperature of all materials remained constant at 298 ± 0.1 K.

Carrier-free recombinant human BDNF (rhBDNF) and carrier-free recombinant human NT3 (rhNT3), collectively referred to as neurotrophins (NTs), were prepared as unfiltered stock solutions with a typical concentration of 250 mg L^{-1} . The lyophilized NTs of known concentrations were dissolved in phosphate-buffered saline (PBS), with a pH of 7.4 ± 0.2 , 0.15 M (Biomed, Lublin, Poland) and stored at -20 °C for a maximum of three months. Before each measurement, the stock solution was diluted to a bulk concentration of 13.2 mg L^{-1} in PBS solution. The exact concentrations of the solutions were determined using a commercially available enzyme-linked immunosorbent (ELISA) assay (DY992, DY990, DY994, DY999, DY995, WA126, DY006, DY268, R&D Systems). The temperature of the experiments was kept constant at 298 ± 0.1 K.

PEG

Poly(ethylene glycol) (PEG), a 4 kDa molar mass (1546569, GMP grade, Sigma Aldrich), was used without further purification to encapsulate NT3-BDNF nanoparticles simultaneously. The working solution of PEG was prepared by aseptically dissolving 2 g of PEG-4000 in 10 mL of Ringer's solution. The mixture was then gently rotated in a tube for 15 min at room temperature. Subsequently, the solution was filtered through a 0.22 μm filter (Millipore), yielding a 200 mg mL^{-1} PEG-4000 working stock, which was further used to prepare PEGylated NT3-BDNF nanoparticles.

Preparation of pegylated NT3-BDNF nanoparticles

PEGylated BDNF-NT3 nanoparticles were prepared at the Pomeranian Medical University in Szczecin. BDNF and NT3 were adsorbed onto the PEG surface through electrostatic interactions. Initially, the hydrodynamic diameter and electrophoretic mobility of PEG molecules in the working solution were determined. Subsequently, NT3 was adsorbed by combining 20 000 mg L^{-1} PEG in the working solution with a 250 mg L^{-1} NT3 suspension at a ratio of 17:1. The mixture was incubated at room temperature for 900 s, resulting in a 13.2 mg L^{-1} final concentration of the NT3 protein in the PEG-NT3 suspension. The hydrodynamic diameter and electrophoretic mobility of the PEG-NT3 nanoparticles were measured, and the corresponding zeta potential was calculated.

Then, 250 mg L^{-1} BDNF was added to the PEG-NT3 suspension at a ratio of 17:1 (PEG-NT3: BDNF). The mixture was incubated at room temperature for another 900 seconds, resulting in a final concentration of 13.2 mg L^{-1} BDNF protein in the PEG-NT3-BDNF mixture. After 1 500 seconds of incubation, spontaneous self-assembly of PEG-NT3-BDNF complexes occurred, referred to as "PEGylated NTs-based nanoparticles" or "PEGylated NT3-BDNF". NTs were mixed with PEG in aqueous solution without further sonication or extensive agitation. PEG chains were conjugated to nanoparticle surfaces via amide or carboxyl bonds, depending on the type of core charge of the amino acids in the protein complex NT3-BDNF and the formation of PEG amino groups and protein amino surface groups. After each component was added, samples were taken to assess the protein concentration using an ELISA. The nanoparticles in PBS's solution were stored at -20 °C for up to two months without any detectable protein loss.

Nanoparticle preparation for in vivo experiments was performed in a controlled laminar-flow hood to ensure sterility of the entire system.

Physicochemical characterization of pegylated NTs nanoparticles

Multiangle dynamic light scattering (MADLS)

A multifaceted approach was used to determine the concentration and size distribution of PEGylated BDNF-NT3 nanoparticles. Particle size analysis was performed using multi-angle dynamic light scattering (MADLS) on a ZetaSizer Ultra instrument (Malvern Instruments, Malvern, UK) equipped with ZS XPLOER 3.2.0 software. The time-averaged scattered intensity from molecular scatterers was recorded to obtain reliable hydrodynamic size distributions. MADLS and conventional dynamic light scattering (DLS) are well-established techniques for determining the hydrodynamic diameter of nanoparticles or macromolecules in dispersion. In particular, MADLS enables accurate characterization of the dispersion and aggregation states of nanomaterials in solution.

The particle size distributions were obtained from the measured diffusion coefficients. The diffusion coefficient of the NPs was determined via DLS using a Zetasizer Nano ZS Malvern instrument at a final concentration of BDNF and NT3 of 13.2 mg L⁻¹, as described previously¹⁶. The data analysis was performed in automatic mode at 25 °C. The measured size is presented as the average value of 20 runs, with triplicate measurements within each run, described in detail elsewhere⁴⁹.

Electrophoretic light scattering (ELS)

The zeta potential and polydispersity index of the PEGylated NT3-BDNF nanoparticles were determined by laser Doppler velocimetry (LDV) at 25 °C with a Malvern ZetaSizer Ultra Particle Analyzer through diffusion coefficient (*D*) and electrophoretic mobility (μ_e) measurements. The LDV method introduced by Adamczyk et al. is based on measuring changes in ζ -potential/microphoretic mobility during the adsorption of tested proteins/particles on a model colloid particle⁵⁰. The electrophoretic mobility was recalculated to the ζ -potential using the Henry equation, which is valid for higher ionic strengths in which the polarization of the electric double layer is relevant (the double-layer thickness decreases as the protein dimension).

Transmission electron microscopy (TEM)

A JEOL JSM-7500 F electron microscope working in transmission mode (TEM) was used to evaluate the morphology and size distribution of the PEGylated NT3-BDNF nanoparticle suspension (in 0.15 M PBS solution). Stock suspensions of nanoparticles (NPs) containing 13.2 mg L⁻¹ BDNF and NT3 proteins were deposited on a copper grid coated with carbon film to prepare the samples for microscopic imaging. After the PBS solution had evaporated, dark and bright field images of the NPs were taken. The micrographs were analyzed using MultiScan 6.08 software (a computer scanning system). All the images represent direct detection from the sample surfaces, with no coating or contrast applied. The size of the PEGylated NT3-BDNF nanoparticles was determined using ImageJ software by gathering the number and coordinates of a minimum of 300 nanoparticles. The counting of PEGylated NT3-BDNF nanoparticle dimensions was a manual process that compared the initial image with a modified version generated by digital image filters. Specifically, the alteration of the picture background was instrumental in this method. By applying these filters, we assessed the accuracy of the particle analysis using the software mentioned above.

Enzyme-linked immunosorbent assay (ELISA)

The concentration of the neurotrophins was measured with immunoenzymatic test ELISA (cat no. DY992, DY990, DY994, DY999, DY995, WA126, DY006, DY248, DY267, R&D Systems, Minneapolis, MN, USA). The test involves the use of immobilized biotinylated antibodies specific to fragments of the investigated protein. After the studied material was applied to the antibody-coated surface, streptavidin-conjugated horseradish peroxidase was added, and the reaction substrate was incubated with the samples at $\lambda = 540$ nm and $\lambda = 450$ nm. The absorbance was read with a Varioskan LUX Plate Reader (Thermo Fisher Scientific, Waltham, MA, USA). The concentration of each protein was determined relative to an appropriate, freshly prepared standard curve (provided with the kit).

Analysis of blood counts, biochemical parameters and CRP level in plasma and cerebrospinal fluid

The analysis of selected biochemical parameters and blood counts on smears from the experimental animals was performed in the accredited veterinary laboratory on samples taken at four time points: before the first administration of cells/NaCl (1), one week after the first administration of cells/NaCl (2), one week after the second administration of cells/NaCl (3), one week after the administration of NTs/NaCl (4). Levels of liver enzymes (AST, ALT) and blood morphological parameters (MCV, MCH, MCHC, hematocrit, hemoglobin content, number per volume unit and the percentage of erythrocytes, platelets, leukocytes, monocytes, neutrophils, basophils, eosinophils) were analysed.

C-reactive protein (CRP) levels were measured in the plasma and cerebrospinal fluid (CSF) of pigs in three research groups: (1) after intrathecal administration of 0.9% NaCl (control group), (2) after intrathecal administration of 5 million ASC, (3) after intrathecal administration of 5 million WJ-MSC. The CRP levels were measured: (1) before the start of the procedure, (2) one week after the first administration of cells/NaCl, (3) one week after the second administration of cells/NaCl, (4) one week after the administration of NTs. A Pig CRP ELISA kit was used (Abcam, #ab205089) was used to determine CRP levels.

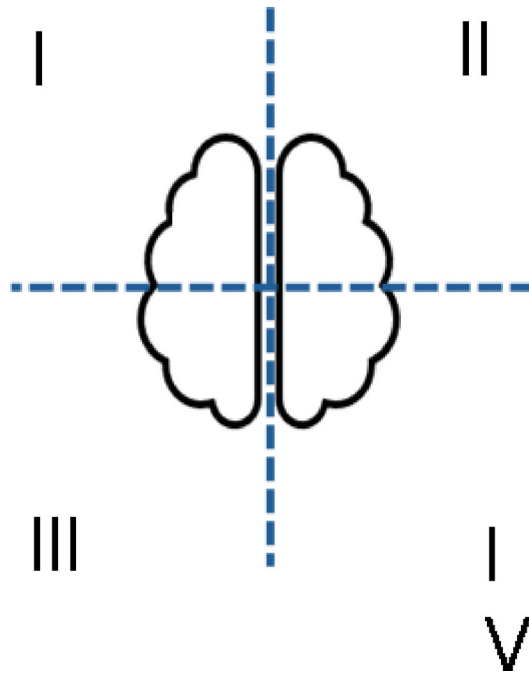


Fig. 11. Scheme of brain division for histochemical analysis. The icons have been sourced from the Microsoft Office stock images, which have been used under licence, and have been modified by the author.

| Sequence | TR (ms) | TE (ms) | FOV (mm ²) | Matrix | Slice thickness (mm) | Gap (mm) | Voxel size (mm ³) | Notes |
|----------------------|---------|---------|------------------------|---------|----------------------|----------|-------------------------------|------------------------------------|
| T2-TSE-COR | 4000 | 100 | 200×200 | 320×320 | 2 | 0.2 | 0.625×0.625×2 | Coronal T2-weighted |
| T2-TSE-SAG | 3500 | 90 | 200×200 | 320×320 | 2 | 0.2 | 0.625×0.625×2 | Sagittal T2-weighted |
| T2-FL2D-SAG-HEMO | 3000 | 80 | 200×200 | 256×256 | 3 | 0.3 | 0.78×0.78×3 | Hematoma-sensitive |
| T2-TSE-TRA | 4000 | 100 | 200×200 | 320×320 | 3 | 0 | 0.625×0.625×3 | Axial T2-weighted |
| T2-SPC-SAG-ISO-1.0MM | 2500 | 85 | 200×200 | 256×256 | 1 | 0 | 1×1×1 | Isotropic high-resolution sagittal |

Table 2. Magnetic resonance imaging sequences and acquisition parameters used for spinal Canal assessment and tracking of iron-labeled cells.

Analysis of MSC biodistribution in the nervous tissue

To assess the biodistribution of mesenchymal stem/stromal cells in the tissues of the experimental animals, the collected tissues were subjected to histochemical analyses. The tissues, fixed in 4% buffered paraformaldehyde and permeated with 30% sucrose, were frozen and cut into 10 µm sections using a cryostat. The brain was divided into 4 sections, according to the diagram below (Fig. 11):

In anticipation of cell migration from the CSF, the preparations were sectioned to obtain samples from the surfaces closest to the areas where CSF circulates. Section I was cut from the side of the cerebral ventricle, section II from the lateral side, section III from the side of the medulla oblongata and section IV from the top. The spinal cord from the lower thoracic sections (at T11) to the cauda equina was dissected together with the nerve roots and divided into sections according to the course of the spinal nerves. The sections were embedded in freezing medium and sectioned in the transverse plane in a caudal direction.

The sections obtained were subjected to topographic staining with haematoxylin and eosin (HE) and trivalent iron staining with 2% potassium ferrocyanide. The preparations were analysed using an Olympus BX51 microscope.

MRI

All animals underwent magnetic resonance imaging (MRI) at four time points: before surgical procedures, after administration of the cell-based product, neurotrophins (NTs), or placebo, and one week after the last procedure, prior to euthanasia. Imaging was performed using a Siemens Magnetom Prisma Fit 3 T scanner equipped with a spine coil. Animals were anesthetized and positioned in the prone position to minimize motion artifacts.

MRI sequences were selected to provide detailed visualization of the spinal canal, detect potential artifacts, and monitor the distribution of iron-labeled cells following intrathecal administration. The acquisition parameters are summarized in Table 2.

Hypointense signals on T2-weighted sequences were used to identify the presence and distribution of iron-labeled cells within the spinal canal.

Statistical analysis

Statistical analysis was performed using GraphPad Prism 10.0 software (GraphPad Software, San Diego, USA). All data are presented as mean \pm standard deviation (SD). Differences between study groups and consecutive time points were assessed using two-way ANOVA, followed by Tukey's multiple comparison test to determine the significance of intergroup differences. Statistical significance was considered achieved at $p < 0.05$. The significance levels are indicated as follows: $p < 0.05$ (*), $p < 0.01$ (**), $p < 0.001$ (***), $p < 0.0001$ (****).

Due to the limited number of animals per group ($n = 3$), the two-way ANOVA was applied in an exploratory manner to identify trends and potential interactions between experimental factors rather than to infer population-level effects. Although the statistical power was limited, this approach is acceptable in preclinical large-animal studies primarily focused on safety assessment and biological response. This analytical approach is consistent with exploratory safety-focused large-animal studies.

Histochemical analysis (assessment of iron ion signal intensity) was descriptive in nature and aimed at identifying areas of the central nervous system containing iron deposits. As stipulated in the study protocol, no statistical evaluation of signal intensity or intergroup comparisons was performed. Instead, the results were presented in the form of qualitative visualizations.

Conclusions

This study evaluated the safety of MSCs combined with neurotrophin-releasing polyelectrolyte nanoparticles as a preclinical ALS therapy. The procedure caused no side effects, and neurotrophins reduced inflammatory markers in cerebrospinal fluid and plasma, suggesting improved efficacy by modulating the CNS microenvironment. Intrathecal administration was safe, and biodistribution analysis showed cell movement within the CNS, around the spinal cord and brain, without crossing the blood-brain barrier. These findings indicate that cell therapy with neurotrophins is a promising alternative to traditional or genetically modified approaches, using readily available autologous or allogeneic cells.

Data availability

Data is provided within the manuscript.

Received: 17 September 2025; Accepted: 11 February 2026

Published online: 27 February 2026

References

- Sabatelli, M., Conte, A. & Zollino, M. Clinical and genetic heterogeneity of amyotrophic lateral sclerosis. *Clin. Genet.* **83**, 408–416 (2013).
- Deda, H. et al. Treatment of amyotrophic lateral sclerosis patients by autologous bone marrow-derived hematopoietic stem cell transplantation: A 1-year follow-up. *Cytotherapy* **11**, 18–25 (2009).
- Witzel, S. et al. Safety and effectiveness of long-term intravenous administration of edaravone for treatment of patients with amyotrophic lateral sclerosis. *JAMA Neurol.* **79**, 121–130 (2022).
- Feldman, E. L. et al. Amyotrophic lateral sclerosis. *Lancet* **400**, 1363–1380 (2022).
- Wang, L. T. et al. Human mesenchymal stem cells (MSCs) for treatment towards immune- and inflammation-mediated diseases: Review of current clinical trials. *J. Biomed. Sci.* **23**, 76 (2016).
- Sironi, F., De Marchi, F., Mazzini, L. & Bendotti, C. Cell therapy in ALS: An update on preclinical and clinical studies. *Brain Res. Bull.* **194**, 64–81 (2023).
- Ciervo, Y. et al. Adipose-derived stem cells protect motor neurons and reduce glial activation in both in vitro and in vivo models of ALS. *Mol. Ther.* **21**, 413–433 (2021).
- Dolezalova, D. et al. Pig models of neurodegenerative disorders: Utilization in cell replacement-based preclinical safety and efficacy studies. *J. Comp. Neurol.* **522**, 2784–2801 (2014).
- Zhu, L., Li, S., Li, X. J. & Yin, P. Pathological insights from amyotrophic lateral sclerosis animal models: Comparisons, limitations, and challenges. *Transl. Neurodegener.* **12**, 46 (2023).
- Crociara, P. et al. Motor neuron degeneration, severe myopathy and TDP-43 increase in a transgenic pig model of SOD1-linked familial ALS. *Neurobiol. Dis.* **124**, 263–275 (2019).
- Yang, H. et al. Species-dependent neuropathology in transgenic SOD1 pigs. *Cell Res.* **24**, 464–481 (2014).
- Zhang, B. et al. DL0410 attenuates oxidative stress and neuroinflammation via BDNF/TrkB/ERK/CREB and Nrf2/HO-1 activation. *Int. Immunopharmacol.* **86**, 106729 (2020).
- Ateaque, S. et al. Selective activation and down-regulation of Trk receptors by neurotrophins in human neurons co-expressing TrkB and TrkC. *J. Neurochem.* **161**, 463–477 (2022).
- The BDNF Study Group. A controlled trial of Recombinant methionyl human BDNF in ALS: the BDNF study group (Phase III). *Neurology* **52**, 1427–1433 (1999).
- Dąbkowska, M. et al. BDNF-loaded PDADMAC-heparin multilayers: A novel approach for neuroblastoma cell study. *Sci. Rep.* **13**, 17939 (2023).
- Dąbkowska, M., Kosiorowska, A. & Machaliński, B. The impact of serum protein adsorption on pegylated NT3-BDNF nanoparticles—distribution, protein release, and cytotoxicity in a human retinal pigmented epithelial cell model. *Pharmaceutics* **15**, 2236 (2023).
- Dąbkowska, M. et al. In vitro and in vivo characterization of human serum albumin-based PEGylated nanoparticles for BDNF and NT3 codelivery. *Int. J. Biol. Macromol.* **265**, 130726 (2024).
- Song, X. Y., Fan, C. X., Rahman, A. U., Choudhary, M. I. & Wang, X. P. Neuro-regeneration or repair: Cell therapy of neurological disorders as a way forward. *Curr. Neuropharmacol.* **22**, 2272–2283 (2024).
- Garbuzova-Davis, S. et al. Multiple intravenous administrations of human umbilical cord blood cells benefit in a mouse model of ALS. *PLoS One* **7**, e31254 (2012).
- Garbuzova-Davis, S. et al. Human umbilical cord blood treatment in a mouse model of ALS: Optimization of cell dose. *PLoS One* **3**, e2494 (2008).
- Terashima, T. et al. Stem cell factor-activated bone marrow ameliorates amyotrophic lateral sclerosis by promoting protective neuroglial migration. *J. Neurosci. Res.* **92**, 856–869 (2014).
- Goutman, S. A., Savelieff, M. G., Sakowski, S. A. & Feldman, E. L. Stem cell treatments for amyotrophic lateral sclerosis: A critical overview of early phase trials. *Expert Opin. Investig. Drugs* **28**, 525–543 (2019).

23. Lunn, J. S., Sakowski, S. A. & Feldman, E. L. Concise review: Stem cell therapies for amyotrophic lateral sclerosis: Recent advances and prospects for the future. *Stem Cells* **32**, 1099–1109 (2014).
24. Atassi, N. et al. attendees of the International Workshop on Progress in Stem Cells Research for ALS/MND. Intraspinial stem cell transplantation for amyotrophic lateral sclerosis: ready for efficacy clinical trials? *Cytotherapy* **18**, 1471–1475 (2016).
25. Feldman, E. L. et al. Intraspinial neural stem cell transplantation in amyotrophic lateral sclerosis: Phase 1 trial outcomes. *Ann. Neurol.* **75**, 363–373 (2014).
26. Kuzma-Kozakiewicz, M. et al. Intraspinial transplantation of the adipose tissue-derived regenerative cells in amyotrophic lateral sclerosis in accordance with the current experts' recommendations: choosing optimal monitoring tools. *Stem Cells Int.* 4392017 (2018). (2018).
27. Mazzini, L. et al. Results from phase I clinical trial with intraspinal injection of neural stem cells in amyotrophic lateral sclerosis: A long-term outcome. *Stem Cells Transl. Med.* **8**, 887–897 (2019).
28. Barczewska, M. et al. Umbilical cord mesenchymal stem cells in amyotrophic lateral sclerosis: An original study. *Stem Cell Rev. Rep.* **16**, 922–932 (2020).
29. Petrou, P., Kassis, I., Yaghmour, N. E., Ginzberg, A. & Karussis, D. A phase II clinical trial with repeated intrathecal injections of autologous mesenchymal stem cells in patients with amyotrophic lateral sclerosis. *Front. Biosci. Landmark* **26**, 693–706 (2021).
30. Riley, J. et al. Intraspinial stem cell transplantation in amyotrophic lateral sclerosis: A phase I trial, cervical microinjection, and final surgical safety outcomes. *Neurosurgery* **74**, 77–87 (2014).
31. Karussis, D. et al. Safety and immunological effects of mesenchymal stem cell transplantation in patients with multiple sclerosis and amyotrophic lateral sclerosis. *Arch. Neurol.* **67**, 1187–1194 (2010).
32. Prabhakar, S. et al. Autologous bone marrow-derived stem cells in amyotrophic lateral sclerosis: A pilot study. *Neurol. India* **60**, 465–469 (2012).
33. Nabavi, S. M. et al. Safety, feasibility of intravenous and intrathecal injection of autologous bone marrow-derived mesenchymal stromal cells in patients with amyotrophic lateral sclerosis: an open label phase I clinical trial. *Cell. J.* **20**, 592–598 (2019).
34. Barczewska, M. et al. Safety of intrathecal injection of Wharton's jelly-derived mesenchymal stem cells in amyotrophic lateral sclerosis therapy. *Neural Regen. Res.* **14**, 313–318 (2019).
35. Staff, N. P. et al. Safety of intrathecal autologous adipose-derived mesenchymal stromal cells in patients with ALS. *Neurology* **87**, 2230–2234 (2016).
36. Berry, J. D. et al. NurOwn, phase 2, randomized, clinical trial in patients with ALS: safety, clinical, and biomarker results. *Neurology* **93**, e2294–e2305 (2019).
37. Shin, S. et al. Comparative proteomic analysis of the mesenchymal stem cells secretome from adipose, bone marrow, placenta and Wharton's jelly. *Int. J. Mol. Sci.* **22**, 845. <https://doi.org/10.3390/ijms22020845> (2021).
38. Oh, K. W. et al. Phase I trial of repeated intrathecal autologous bone marrow-derived mesenchymal stromal cells in amyotrophic lateral sclerosis. *Stem Cells Transl. Med.* **4**, 590–597 (2015).
39. Cudkovic, M. E. et al. A randomized placebo-controlled phase 3 study of mesenchymal stem cells induced to secrete high levels of neurotrophic factors in amyotrophic lateral sclerosis. *Muscle Nerve* **65**, 291–302 (2022).
40. Kim, T. H. et al. Tracking of transplanted mesenchymal stem cells labeled with fluorescent magnetic nanoparticle in liver cirrhosis rat model with 3-T MRI. *Magn. Reson. Imaging* **28**, 1004–1013 (2010).
41. Daldrup-Link, H. E. et al. Targeting of hematopoietic progenitor cells with MR contrast agents. *Radiology* **228**, 760–767 (2003).
42. Kraitchman, D. L. et al. In vivo magnetic resonance imaging of mesenchymal stem cells in myocardial infarction. *Circulation* **107**, 2290–2293 (2003).
43. Hauger, O. et al. W. MR evaluation of the glomerular homing of magnetically labeled mesenchymal stem cells in a rat model of nephropathy. *Radiology* **238**, 200–210 (2006).
44. Markides, H. et al. Ex vivo MRI cell tracking of autologous mesenchymal stromal cells in a bovine osteochondral defect model. *Stem Cell. Res. Ther.* **10**, 25 (2019).
45. Kim, T. et al. Mesoporous silica-coated Hollow manganese oxide nanoparticles as positive T1 contrast agents for labeling and MRI tracking of adipose-derived mesenchymal stem cells. *J. Am. Chem. Soc.* **133**, 2955–2961 (2011).
46. Ende, N., Weinstein, F., Chen, R. & Ende, M. Human umbilical cord blood effect on SOD mice (amyotrophic lateral sclerosis). *Life Sci.* **67**, 53–59 (2000).
47. Habisch, H. J. et al. Intrathecal application of neuroectodermally converted stem cells into a mouse model of ALS: limited intraparenchymal migration and survival narrows therapeutic effects. *J. Neural Transm (Vienna)* **114**, 1395–1406 (2007).
48. Dąbkowska, M. et al. Electrostatic complex of neurotrophin 4 with dendrimer nanoparticles: controlled release of protein in vitro and in vivo. *Int. J. Nanomed.* **14**, 6117–6131 (2019).
49. Dąbkowska, M., Adamczak, M., Barbasz, J., Cieśla, M. & Machaliński, B. Adsorption/desorption transition of recombinant human neurotrophin 4: Physicochemical characterization. *Langmuir* **33**, 9548–9557 (2017).
50. Dąbkowska, M.; Adamczyk, Z.; Cieśla, M.; Adamczak, M.; Bober, J. Lysozyme Monolayers at Polymer Microparticles: Electrokinetic Characteristics and Modeling. *J. Phys. Chem. C* **2018**, **122** (36), 20777–20788. DOI:<https://doi.org/10.1021/acs.jpcc.8b04916>.

Author contributions

KJW, AS, and BM conceived the study concept and design; MD, JSCh, DM, ID, MChM, and MR conducted the experiments; PH and ID managed the pig herd, performed animal procedures, and assessed disease symptoms; KJW, MM, AS, and EP analyzed the data; and ES and KJW wrote the manuscript. All authors read, edited, and approved the final version of the manuscript.

Funding

This research was funded by the Medical Research Agency, Poland (No: 2020/ABM/01/00014–00). The clinical procedures and histopathological analyses were conducted at the Regenerative Medicine Laboratory of the Faculty of Medicine, Medical College of the University of Warmia and Mazury in Olsztyn. Funded by the Minister of Science under "the Regional Initiative of Excellence Program".

Declarations

Competing interests

The authors declare no competing interests.

Additional information

Correspondence and requests for materials should be addressed to K.J.-W.

Reprints and permissions information is available at www.nature.com/reprints.

Publisher's note Springer Nature remains neutral with regard to jurisdictional claims in published maps and institutional affiliations.

Open Access This article is licensed under a Creative Commons Attribution-NonCommercial-NoDerivatives 4.0 International License, which permits any non-commercial use, sharing, distribution and reproduction in any medium or format, as long as you give appropriate credit to the original author(s) and the source, provide a link to the Creative Commons licence, and indicate if you modified the licensed material. You do not have permission under this licence to share adapted material derived from this article or parts of it. The images or other third party material in this article are included in the article's Creative Commons licence, unless indicated otherwise in a credit line to the material. If material is not included in the article's Creative Commons licence and your intended use is not permitted by statutory regulation or exceeds the permitted use, you will need to obtain permission directly from the copyright holder. To view a copy of this licence, visit <http://creativecommons.org/licenses/by-nc-nd/4.0/>.

© The Author(s) 2026